Fragility Analysis of Pile-Supported Wharves in the Cascadia Subduction Zone

By

Ahmad Sepehri Sefidab

A Thesis Submitted in Partial Fulfillment
of the Requirements for the Degree of

MASTER OF APPLIED SCIENCE

in the Department of Civil Engineering

University of Victoria

Fragility Analysis of Pile-Supported Wharves in the Cascadia Subduction Zone

By

Ahmad Sepehri Sefidab
MASc., University of Victoria, 2021

Supervisory Committee

Dr. Lina Zhou, Department of Civil Engineering

Co-Supervisor

Dr. Cheng Lin, Department of Civil Engineering

Co-Supervisor

Dr. Tuna Onur, Department of Civil Engineering

Departmental Member

Abstract

In this study, incremental dynamic analyses were carried out to investigate the damage risk of a typical pile-supported wharf under three types of ground motions that may happen in the Cascadia Subduction Zone, i.e., the shallow crustal, in-slab, and interface earthquakes. Firstly, a prestressed concrete pile-supported wharf located in Vancouver, site class C, was designed according to the displacement-based design approach recommended by ASCE 61 (2014). Next, a two-dimensional nonlinear numerical model of the wharf was created in OpenSees software. The fiber section method was used in this research to simulate the plastic performance of piles. Soil-structure interaction was implemented using three types of nonlinear springs available in the OpenSees library. The nonlinear modeling method of pile-deck connections was validated with experimental results from past research. For nonlinear dynamic analyses, eleven ground motions (two horizontal components per motion) were selected for each type of earthquake following a series of selection criteria. After that, incremental dynamic analyses (IDA) were performed that include thousands of nonlinear calculations in total. Three damage states represented by the strain limit of materials were defined based on criteria proposed in PIANC (2001). Finally, three sets of fragility curves were developed for each type of ground motion as a cumulative distribution function of spectral accelerations, representing the probability of occurrence of three different damage states: serviceable damage, repairable damage, and severe damage. Results show the importance of considering in-slab and shallow crustal events for wharf structures located in the Cascadia Subduction Zone. For the hazard level with an exceedance of 2% in 50 years, the risk of serviceable damage on pile-supported wharves located in Vancouver under all three types of earthquakes is fairly high, while the risk of repairable and severe damage is acceptable. In general, interface earthquakes are not the significant earthquakes for wharves located in Vancouver (or lower mainland). This is due to the large distance of Vancouver to the rupture area which damps high-frequency motions (shorter periods), and makes short-period structures, such as wharves analyzed in this project, less vulnerable to these earthquakes. Based on deaggregated hazards, for the first two damage states, in-slab earthquakes can be considered as the dominant risk for wharves in the lower mainland, while shallow crustal earthquakes are more significant in terms of severe damage. Also, it was found that pulse-like shallow crustal earthquakes should be considered for port structures located in the Cascadia Subduction Zone, as they can have a severe effect on the seismic

performance of port structures and may cause considerable damage to them. This is in response to the uncertainty of the existence of any crustal faults underneath or close to Metro Vancouver.

Table of Contents

List of Figures

List of Tables

Acknowledgments

I would like to thank my supervisor, Dr. Lina Zhou, co-supervisor, Dr. Cheng Lin, and supervisory committee member, Dr. Tuna Onur , for the guidance and support they gave me along with the development of this thesis. I also wish to express my gratitude to Marine Environmental Observation Prediction & Response Network (MEOPAR) since this project was a part of the SIREN project (Strategic Planning for Coastal Community Resilience to Marine Transportation Disruption) funded by MEOPAR.

Chapter 1: Introduction

1.1 Port Structures

Port structures are among the most critical infrastructures in logistical systems, facilitating national and international trade. Functionality and safety of port structures are of utmost importance, especially after seismic events, since any downtime and reduced throughput from seismic damage in ports might result in a significant interruption in the supply of goods and losses for communities and port stakeholders. Therefore, during seismic events, the sustainability and immediate recovery of port structures are crucial for the continued operation of transportation, supply, and trade. An estimation for the level of damage that port structures would experience in earthquakes is vital from a crisis-management perspective. One of the most common types of port structures, especially in marine trading, is pile-supported wharves, which were analyzed in this project. Figure 1-1 shows the seismic risk assessment framework of port systems. As can be seen, structural seismic risk evolution is a key part of the overall process, which is the basis for any further operation and system performance risk prediction.

Meanwhile, the west coast of Canada is the most earthquake-prone region in Canada, with more than 1000 earthquakes being recorded every year, while the majority of these events have a magnitude of less than 3.0. From the offshore region to the west of Vancouver Island, more than 100 earthquakes of magnitude 5 or greater have occurred during the past 70 years (NRCan). The Cascadia Subduction Zone itself can generate massive scale earthquakes, affecting both short-period and long-period structures on the west coast of Canada.

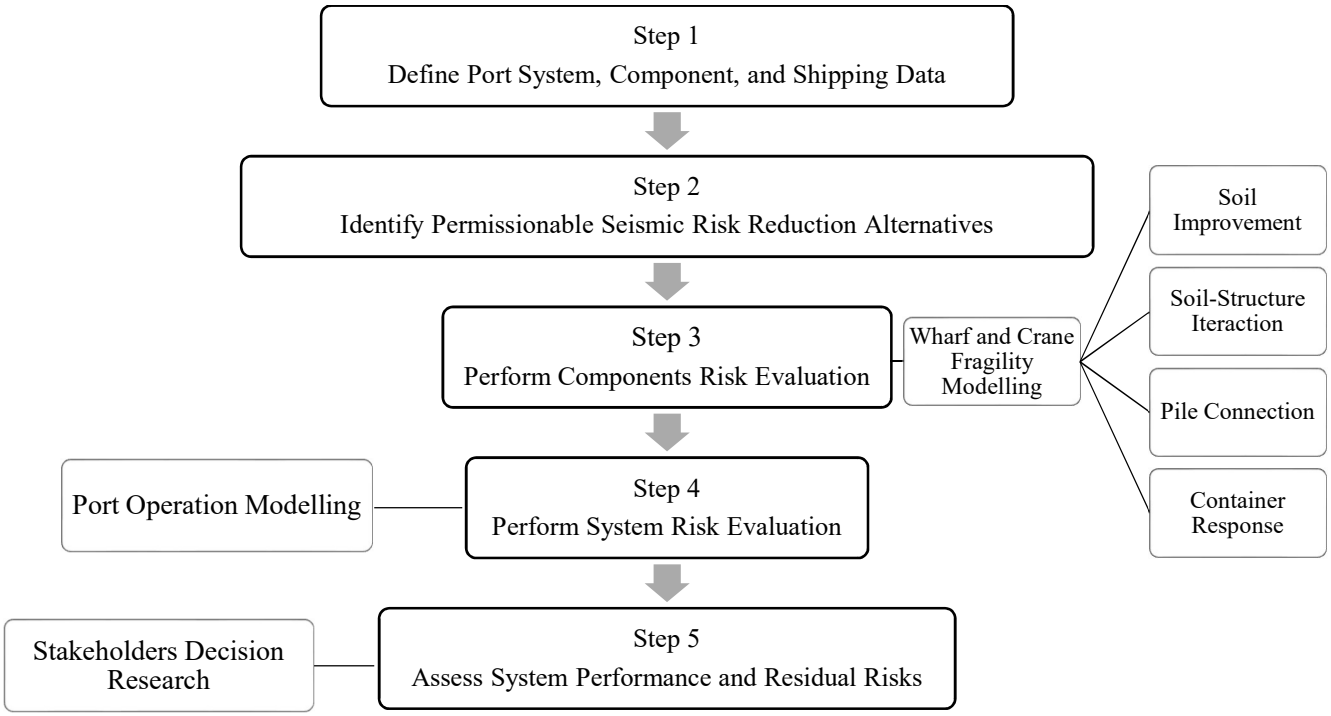

Figure 1-1 Port systems risk assessment framework (Werner et al. 2008)

1.2 Damage of Wharves in Previous Earthquakes

Seismic events pose a significant threat to the Western part of Northern America, where large-magnitude events were recorded. During past earthquakes, port structures experienced significant damage and interruption. For instance, in Loma Prieta 1989 earthquake, several port facilities experienced different levels of damage, such as settlement and pavement damage at Port of Oakland (Kayen et al. 1998). In addition to mobility problems of cranes, which led to limited operation and lateral spreading, damage occurred at the top of several piles at the pile-deck connection zone.

Ben Nutter Terminal Wharf, Berths 35-37 after the Loma Prieta earthquake experienced severe damage, mostly concentrated in pile-deck connection zone, like spalling off of cover concrete. After this earthquake, the crushing of core concrete due to extensive bending demand was observed (Figure 1-2).

Figure 1-2 Damage at a pile-deck connection, Loma Prieta earthquake 1989; Ben Nutter Terminal Wharf, Berths 35 – 37. (Serventi et al. 2004)

In other parts of the world, the Hyogo-ken Nanbu earthquake, which occurred in Japan in 1995, with a magnitude of 6.9, caused damage to the Kobe port (Figure 1-3) (Kayen et al. 1998, Nakahara et al. 2000). The main cause of this considerable damage was the liquefaction of the loose saturated soil layer beneath the port. Buckling failure of the piles was observed at the pile heads and buried segments of those piles.

Substantial damage was induced to Izmit Bay port due to the Kocaeli event, with a magnitude of 7.4 (Erdik 2000). Damage comprised failure of piers, failure of nonstructural equipment, and collapse of some cranes. Also, Derince Port, Turkey, which is a caisson type port structure with a length of about 1.5 km, translated away from the wharf about 70 cm horizontally due to post-earthquake geotechnical problems in Kocaeli event.

Most recently, after the Haiti earthquake, 2010, Port-au-Prince experienced different levels of failure at the pile-supported wharf. The frontage of the main wharf was completely collapsed, which caused a crane to be thrown into the water (Figure 1-4) (Werner et al. 2011).

Figure 1-3 Lateral displacement of a quay wall on Port Island, Kobe 1995. (Werner et al. 2011)

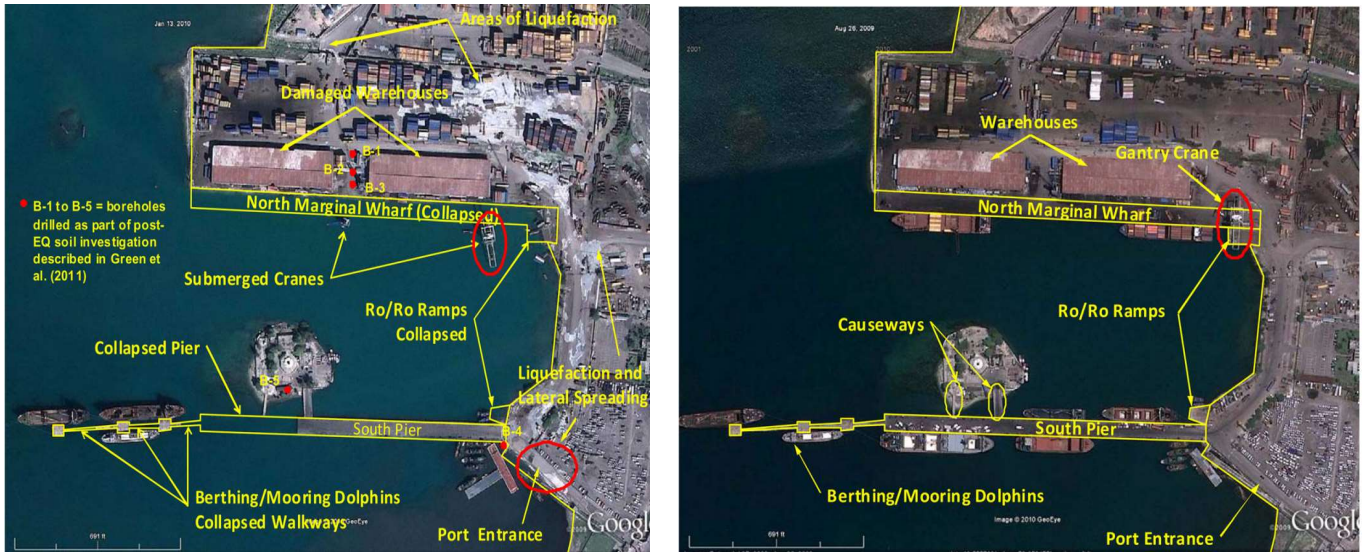

Figure 1-4 Port de Port-au-Prince configuration and facilities before and after the earthquake. (Werner et al. 2011)

Figure 1-5 shows the damages induced by the Great Hanshin earthquake in 1995 to a pile-supported wharf in Kobe Port of Japan. Some piles of the wharf were extracted after the earthquake. The dike movement caused a considerable lateral displacement of the wharf and plastic hinges developed on pile-deck connections and within the embedded part of piles (PIANC 2001).

Figure 1-5 Damage to piles at Takahama Wharf, Kobe Port (after extraction for inspection). (PIANC 2001)

1.3 Research on Seismic Performance of Port Structures

A lot of research has been done on the seismic performance of wharves, to enhance the overall seismic behavior of port structures and reduce the seismic risk. Yang et al. (2012) investigated the seismic risk of vertical-pile-supported wharf commonly used in the western U.S. through developing fragility curves for different damage states under a suite of California ground motions. It was found that implementing container cranes in the analysis can increase the horizontal displacement of the wharf by a rough value of 10%. A 3D nonlinear finite element model (FEM) in OpenSees was developed to study the effect of soil deformation by Su et al. (2017). It was concluded that the soil deformation has a significant effect on the overall behavior of pile-supported wharves. The seismic behavior of a marginal wharf was assessed by developing a 2D numerical model (Shafieezadeh et al. 2009). In this model, the soil liquefaction effect was taken into account. Large deformations were developed under intense seismic load, due to movements of the soil surrounding the piles, which led to damage of pile-deck connections. (Shafieezadeh et al. 2012). Heidary-Torkamani et al. (2014) investigated the different engineering demand parameters (EDP): displacement ductility factor, differential settlement of deck and landside surface, and residual horizontal translation. In this study, three different damage state levels of

Degree I serviceable, Degree II repairable, and Degree III near-collapse were introduced, and related fragility curves were developed. The seismic behavior of marginal wharves, both conventional ones and those with enhanced damage-resisting connections were investigated by Chiaramonte et al. 2013. They found the wharves with controlled rocking connections had a better performance compared to the ones with conventional details.

Further, using FLAC software (reference), nonlinear time history analysis was employed to develop fragility curves for a typical pile-supported wharf in the west coast of United States using ground motions with different hazard levels (Na et al. 2009). In this study, the damage levels were defined based on PIANC (PIANC 2001). Fragility curves were developed based on two different approaches, deterministic and probabilistic. It was concluded that the deterministic model with mean soil parameter values provides a lower probability of failure (underestimation of vulnerability) than the probabilistic model. In another study, seismic fragility curves were derived using finite element analysis in PLAXIS environment for the sheet pile wharves of the Hualien Harbor in Taiwan (Ko et al. 2010). Damage criteria were based on the displacement at the top of sheet piles (PIANC 2001). The effect of different source of geotechnical and structural uncertainties of a pile-supported wharf was investigated through conducting sensitivity analysis employing on IDA approach (Heidary et, al, 2013). It was found that two geotechnical parameters of friction angle and porosity of rock fill, and also dead load, regarded as the structural parameter, affected the seismic performance of the structure most.

In 2011, Chiou et al. proposed a simplified approach to develop fragility curves for the port of Taiwan implementing the Capacity Spectrum Method (CSM). To assess the seismic performance of the port, the fragility curves of the wharf were constructed through simple statistical analysis. 3D responses of the wharf were also investigated during a far-field seismic event (Shafieezadeh et. al, 2013). By applying far-field ground motions, it was found that the 3D model produced very close transverse and vertical responses to the corresponding responses from the 2D model. Also, a comparison of the results showed that the responses of the wharf, like deck displacement, pile-deck connection rotation, and pile section curvature are large enough to consider during the near-field events, while these responses are negligible during the far-field earthquakes.

1.4 Objectives and Methodology

Port structures located in Cascadia Subduction Zone may experience three types of earthquakes: shallow crustal, in-slab, and interface. In the previous studies, the seismic risk of port structures was mainly assessed under shallow crustal earthquakes, while in-slab and interface earthquakes were rarely considered. Different types of ground motions may result in different seismic responses of port structures due to the different characteristics of ground movements, such as frequency content, duration, intensity, distance, pulse effect, etc. Therefore, the objective of this study is to provide an insight into the risk of seismic damage of pile-supported wharves located in the Cascadia Subduction Zone, through developing fragility curves for three types of seismic events that are specific to this region.

In this research, a concrete pile-supported wharf was assumed to be located in Vancouver harbor, BC (soil type C), and designed based on ASCE-61 (2014), a standard commonly used in practice for seismic design of piers and wharves in Canada. A 2D nonlinear finite element model of the wharf was developed in the OpenSees platform. In the numerical models, soil-structure interaction was simulated with soil springs connected to the piles. The nonlinear behavior of the prestressed piles was modeled using the fiber section technique available in OpenSees. Furthermore, the pile-deck connection models were validated with experimental results from reference (Jellin, 2008). The seismic response of the wharf model was investigated through nonlinear time-history analysis under 66 horizontal motion components that cover three types of earthquakes: shallow crustal, in-slab, and interface events. The limit states used in this study to develop fragility curves are based on the strain limits provided by Permanent International Association Navigation Congresses (PIANC) and categorized as Serviceable Damage, Repairable Damage, and Severe Damage. Finally, an incremental dynamic analysis (IDA) procedure was employed to develop the seismic fragility curves of the wharf on three damage levels and under three types of ground motions.

1.5 Thesis Outline

In Chapter 1, the importance of seismic risk assessment of port structures is explained, then followed by a review of port structures damaged in past earthquakes and previous studies on seismic performance of port structures. Chapter 2 describes the details and configurations of the wharf analyzed in this project, the nonlinear modeling method in OpenSees software, and the definition of damage state levels. Chapter 3 discusses the selection and processing methods of ground motions used for nonlinear dynamic analysis. In Chapter 4, incremental dynamic analysis, development of fragility curves, and discussion on results are explained. Conclusions are summarized in Chapter 5. Also, the seismic design of a pile-supported concrete wharf is included in Appendix A.

Chapter 2: Nonlinear Modeling of a Wharf

2.1 Wharf Configuration

Configuration and geometry of the selected wharf are presented in Figure 2-1. The pile-supported wharf is composed of a deck supported by a set of piles, which provide both vertical and lateral resistance for the whole system. The wharf in the transverse direction acts as a moment-resisting frame supported by the soils through soil-pile interactions. The deck is made from prestressed concrete that can provide a high stiffness in both in-plan and out-of-plane directions. The pile-deck connection can be regarded as a moment connection. The dimensions and reinforcement of piles were designed seismically according to ASCE 61 (2014), which is a common practice in Canada, since there is no Canadian standards and guidelines available regarding design of port structures. Detailed design calculations are provided in Appendix A.

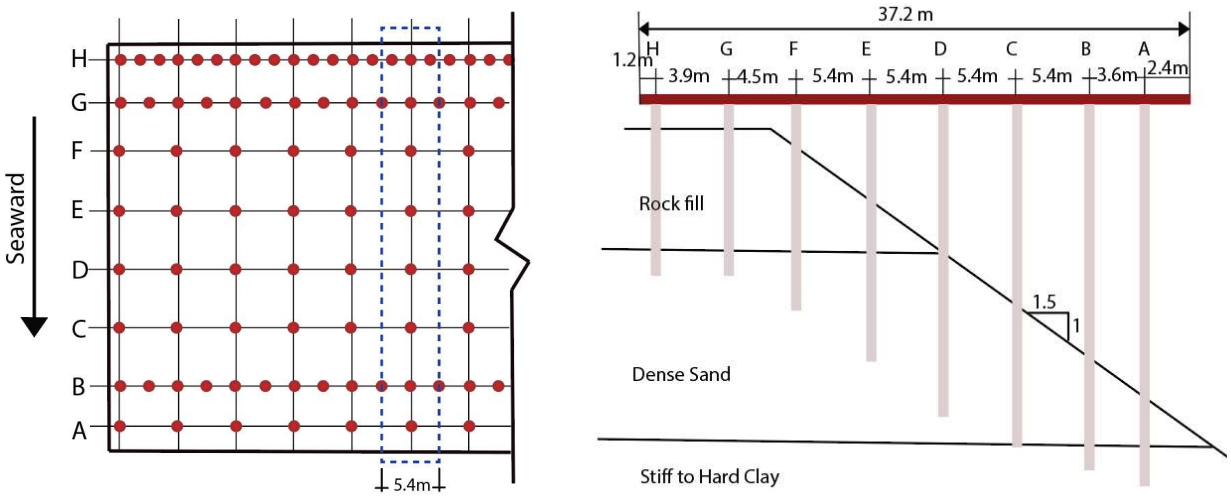

(a) (b)

Figure 2-1 Profile of a wharf: a) plan view; b) section view. (Yang et al. 2012)

2.1.1 Deck

The thickness of the concrete deck is 60 cm, which possesses a massive flexural strength and stiffness relative to the other structural components of the wharf. Therefore, in OpenSees, the deck was modeled with an "elasticBeamColumn" element, and the input parameters were calculated based on material properties and cross-section dimensions.

2.1.2 Piles

Generally speaking, piles can be driven into soils with different orientations, vertically or with an angle, and are categorized as vertical piles or batter piles, respectively. In the former case, the lateral resistance is provided by the bending behavior of piles, while in the latter case, it is provided by both axial and bending behavior of batter piles. The wharf structure analyzed in this study is assumed to be only supported by vertical piles with an octagonal cross-section of 0.61 m (24 in) (Figure 2- (a) and (b)). It is worth noting that the octagonal cross-section saves more materials than the traditional square piles.

There were 12 prestressed strands (nominal diameter of 15.24 mm) distributed in the cross-section of piles (Figure 2- (a)). The strand material was ASTM A416 Grade 270 with yielding stress of 1860 MPa (270 ksi). The compressive strength of concrete was 41.4 MPa (6 ksi). Piles and the concrete deck were connected with dowels that were made of ASTM 416 grade 60 (Figure 2- (b)). A total of 6-#8 (nominal diameter of 25.4 mm) welded head dowel rebars were assigned for pile rows A~F, and 6-#10 (nominal diameter of 32.26 mm) for piles rows G & H. The extended length of #8 and #10 rebars into piles were 1.8 m and 2.2 m, respectively. The detailed design of piles is described in Appendix A.

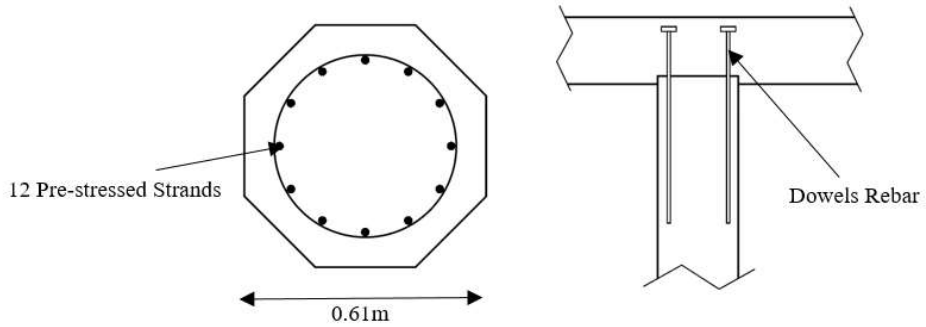

Figure 2-2 Pile details: (a) pile geometry section; (b) T-head dowels in pile connection.

The prestressed concrete piles were modeled using "dispBeamColumn" element in the OpenSees library. It is a nonlinear element controlled by a displacement formula, where the fiber-section modeling technique was adopted. In this model, the cross-section of the pile is divided into a large number of fibers. Through the integration of uniaxial stress-strain behavior assigned to

each fiber, the overall nonlinear behavior of a section can be obtained. Five integration points were assigned for each "dispBeamColumn" element (Figure 2-2).

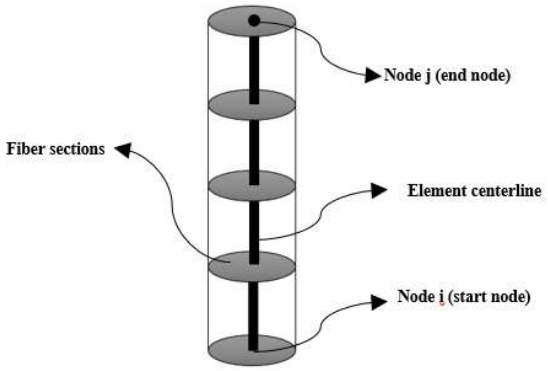

Figure 2-2 Nonlinear model of pile element in OpenSees.

To simplify the modeling procedure, the octagonal cross-section of piles was modeled as a circular cross-section in OpenSees with equivalent mechanical properties (Figure 2-3). Therefore, the circular-shaped mesh can be used for steel and concrete materials.

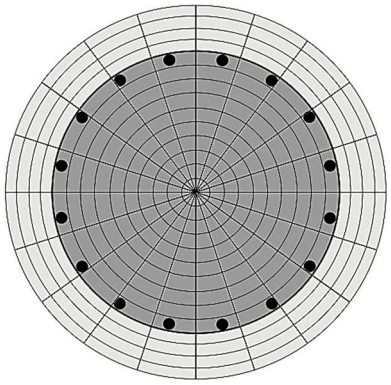

Figure 2-3 Nonlinear fiber-section model.

There are a few concrete material models available in the OpenSees library which can be used for different modeling purposes. In this project, the "Concrete 02" material model was used to model the stress-strain relationship for both unconfined cover concrete and confined core concrete. Table 2-1 list the input parameters for both concrete materials used in this project. The nonlinear stress-strain behavior of concrete material is presented in Figure 2-4 and the definition of each parameter is listed in Table 2-2.

Table 2-1 Concrete properties in OpenSees (Shafieezadeh 2011)

	Confined core concrete	Unconfined cover concrete
Compressive strength at 28 days, f_c	41.4 MPa (66 MPa(1))	41.4 MPa (66 MPa)
Ratio of maximum to nominal strength, K_{fc}	1.54	1.0
Maximum compressive strength, $f_{cc} = K_{fc}f_c$	63.8MPa (101.64 MPa)	41.4 MPa (66 MPa)
Elastic modulus, E_c	30441.7 MPa	30441.7 MPa
Strain at maximum strength	0.0074	0.002
Ratio of ultimate to maximum strength, K_{res}	1.16	0.1
Ultimate compressive strength, $f_{cu} = K_{res}f_{cc}$	74 MPa (66 MPa)	4.14 MPa (6.6 MPa)
Strain at crushing strength	$4.42\varepsilon_{c0}$	0.005
Ratio between unloading slope at $\boldsymbol{\varepsilon_{cu}}$ and initial slope	0.5	0.5
Tensile strength, $f_t = 0.1fcc$	6.38 MPa (10.2 MPa)	4.14 MPa (6.6 MPa)
Tension softening stiffness, $0.1E_c$	3044.17 MP	3044.17 MP

(1) Values used in the verification model (Section 2.2).

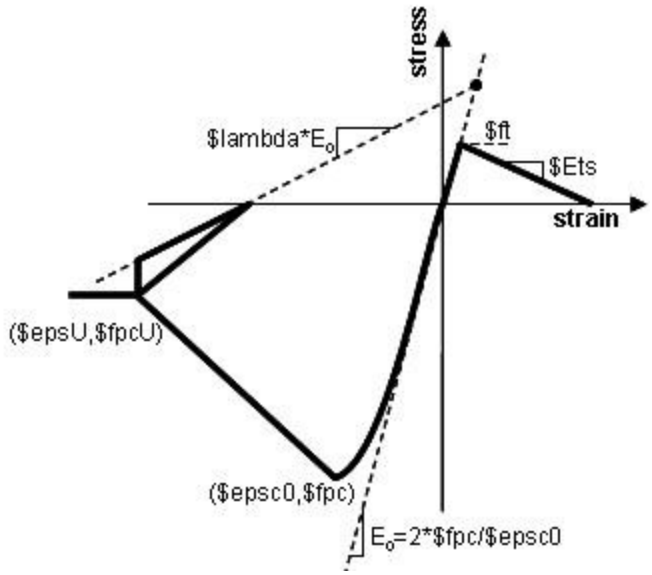

Figure 2-4 Stress-Strain curve of "Concrete 02" material. (OpenSees)

Table 2-2 Definition of parameters in Figure 2-4.

f_pc	concrete compressive strength at 28 days (compression is negative)
eps_c0	concrete strain at maximum strength
f_pcu	concrete crushing strength
eps_U	concrete strain at crushing strength
$lambda	ratio between unloading slope at $epscu and initial slope
f_t	tensile strength
E_ts	tension softening stiffness (absolute value) (slope of the linear tension softening branch)

For modeling prestressed strands in piles, "InitStressMaterial" was utilized to simulate the initial prestress of strands. The stress-strain behavior for this material was defined as "Steel02" (Figure 2-5). The properties of the prestressing strands are listed in Table 2-3. The prestress force is 140 KN, resulting in a service prestress of 9.7 MPa

Table 2-3 “Steel02” material properties in OpenSees. (OpenSees)

Yield stress of steel, $\mathbf{f_y}$	$\mathbf{1860\ MPa\ (270\ ksi)}$
Modulus of elasticity of steel, $\mathbf{E_s}$	$196500\ \text{MPa}\ (8.5 \times 10^6\ \text{ksi})$
Parameters to control the transition from elastic to plastic branches (Recommended by OpenSees)	$R_0 = 10$ $cR_1 = 0.925$ $cR_2 = 0.15$
Strain-hardening ratio for ASTM A416, $\mathbf{B_S}$	0.0087

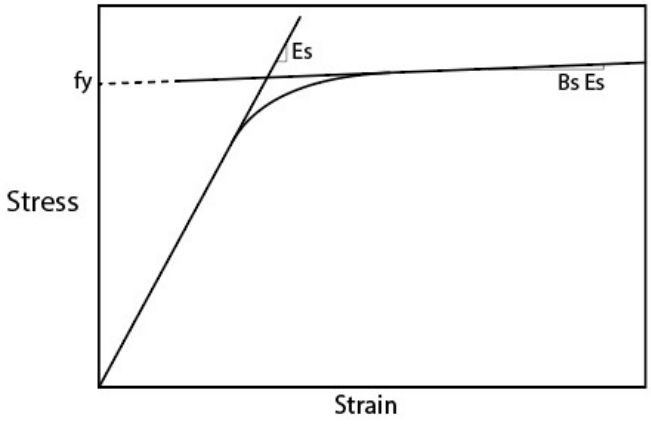

Figure 2-5 “Steel02” material. (OpenSees)

"ReinforcingSteel" was used to model the dowel rebars in the connection zone. This material model can capture and simulate a wide range of rebar failures, such as the Coffin-Manson fatigue, strength reduction, and isotropic hardening, etc. The material used for rebars is ASTM A706 Grade 60 and the parameters of the "ReinforcingSteel" model are shown in Table 2-4. These parameters were obtained based on the fitting process described in the next section. In Table 2-4, parameter $\boldsymbol{\alpha}$ is used to relate damage from one strain range to another strain range, which commonly is a constant value for a specific material. Parameter C_f is the ductility constant that affects the number of cycles to failure of the material. A higher value of C_f leads to lower damage for each cycle. Parameter C_d is the strength reduction constant. A larger C_d leads to a lower reduction of strength for each cycle. The Coffin-Manson fatigue model parameters have been adjusted so that the cyclic degradation of the model can be adequately verified. The verification is discussed in the following section.

Table 2-4 "ReinforcingSteel" material properties in OpenSees.

Yield stress of steel, $\boldsymbol{f_y}$	**410 Mpa (60 ksi)**
Ultimate stress of steel, $\boldsymbol{f_u}$	500 MPa
Modulus of elasticity of steel, $\boldsymbol{E_s}$	210000 MPa
Coffin-Manson constant, $\boldsymbol{C_f}$	0.26
Coffin-Manson constant, $\boldsymbol{\alpha}$	0.5
Cyclic strength reduction constant, $\boldsymbol{C_d}$	0.26

2.2 Pile-deck Connection Model

Based on observations on failure modes of wharves in earthquakes, pile-deck connections are one of the most vulnerable locations for pile-supported wharves. Figure 2-6 shows the details of one of the most common types of pile-deck connections, the T-headed dowel bar connection, which was implemented in this research.

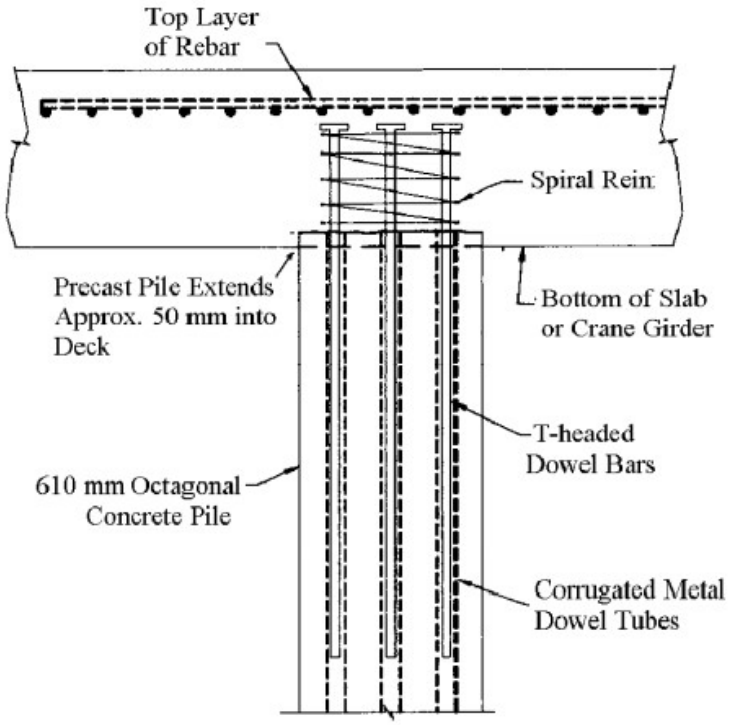

Figure 2-6 T-headed dowel bar connections. (Lehman et al. 2013)

According to Lehman et al. (2013), axial loads have a significant effect on the seismic behavior of pile head connections. The presence of axial loading will reduce the number of cycles that a pile-deck connection can undergo before losing its resistance or complete damage. Figure 2-7 shows the comparison of hysteretic behavior of a pile-deck connection with and without including the axial load.

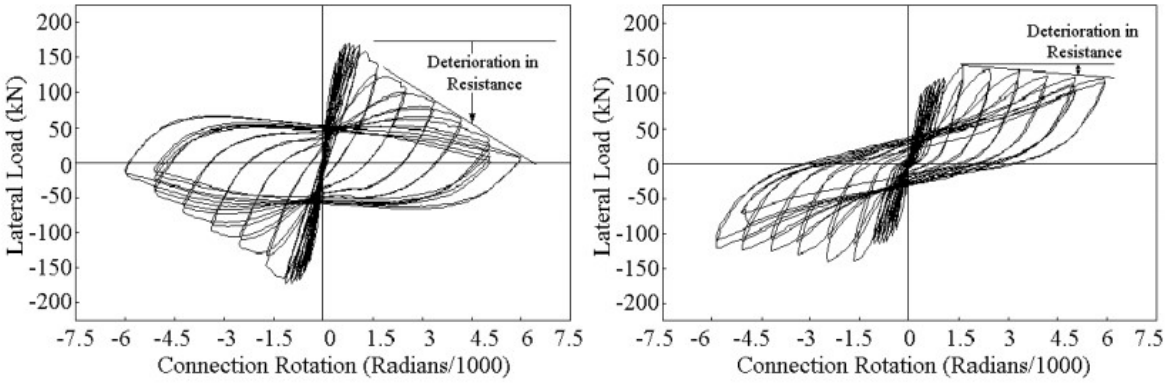

(a) (b)

Figure 2-7 Effect of axial loading on hysteretic behavior of pile-deck connection; a) with axil load; b) without axial load. (Lehman et al. 2013)

In this research, a T-headed dowel connection was implemented. The experimental test results conducted at the University of Washington were employed to verify the numerical modeling approach of pile-deck connections in OpenSees (Jellin 2008). The tested specimen was composed of a 610 mm octagonal precast prestressed concrete pile, connected to a concrete slab with T-head dowels. Prefabricated holes were left in the concrete material and filled with epoxy after the installation of dowels. Reversed cyclic lateral loads were applied to the pile with an increased displacement amplitude. At the same time, the specimen was subjected to a constant axial load, 10% of the axial load capacity of the pile, $0.1f_cA_g$, to account for the effect of gravity loads, where A_g is the gross cross-section area of the pile, and f_c is the specified compressive strength of concrete (Lehman et al. 2013). The pile was reinforced with twenty-two 13 mm diameter low-relaxation strands with a strength of 1860 MPa. The prestress force was 140 KN, resulting in a service prestress of around 9.7 MPa. The concrete compressive strength used the average 28-day concrete compressive strength of 66 MPa. The dowel used to connect pile head to concrete slab was 8-# 10 (32M) ASTM A706 grade with a minimum yield stress of 410 MPa. The specimen setup is shown in Figure 2-8. Figure 2-9 shows the comparison of the force-rotation response of connections derived from numerical modeling developed in this study (red line) versus the experimental test results (black line). As can be seen, the connection model developed in this project can meet well with the test data in terms of strength, stiffness, and cyclic degradation. Material properties used for verification of pile-deck connection are listed in Table 2-1 to Table 2-4.

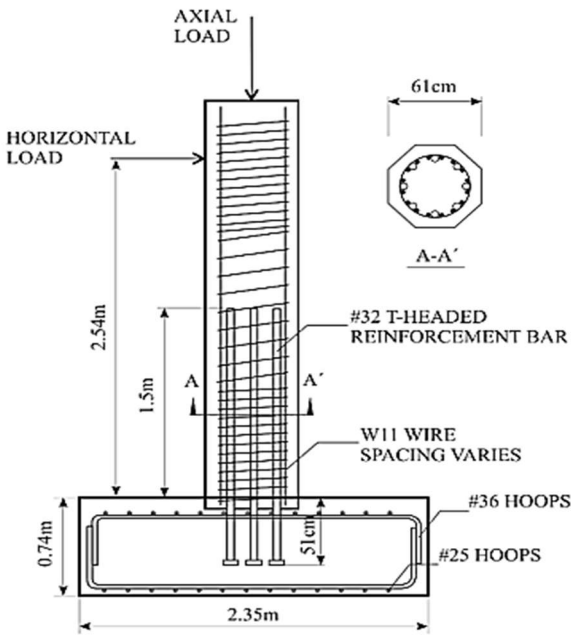

Figure 2-8 Pile to deck connection specimen setup. (Lehman et al. 2013)

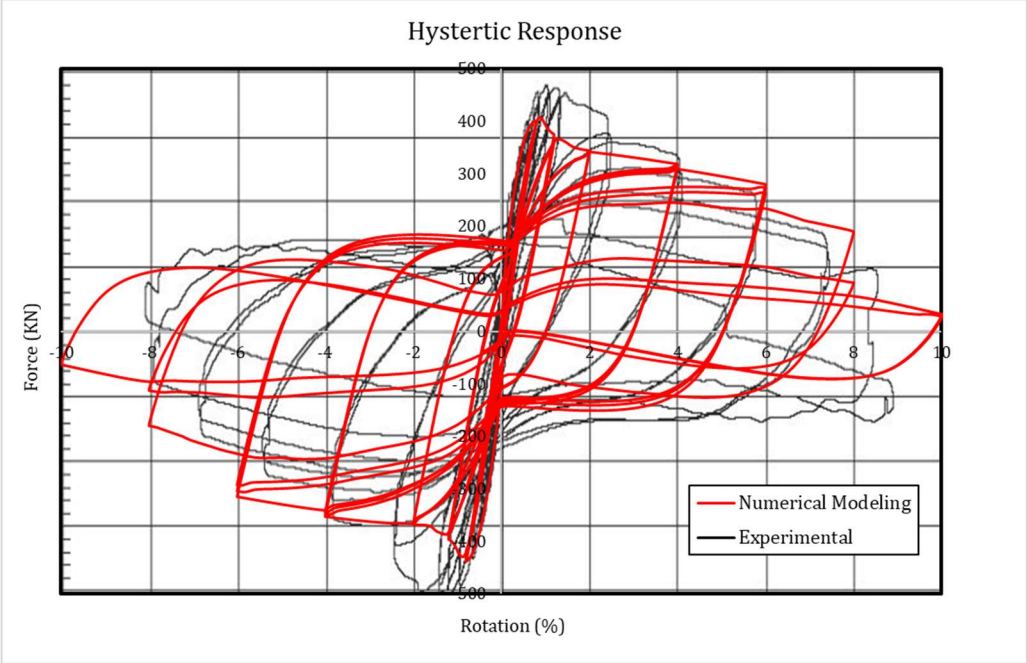

Figure 2-9 Comparison of hysteresis loops of test data and numerical modeling analysis.

2.3 Soil-Structure Interaction

Soil-structure interaction (SSI) has a significant effect on the overall performance of pile-supported structures, especially during seismic events (Su et. Al 2019). The interaction between piles and soils can be modeled by a series of nonlinear soil springs. These springs are commonly named p-y, t-z, and q-z. Lateral stability is provided by p-y springs, which affects the response of the structure most. "PySimple1*"* material is available in the OpenSees library to capture the effects of surrounding soils and was used to simulate lateral (horizontal) stiffness and strength of the soil. All three springs are presented in Figure 2-10.

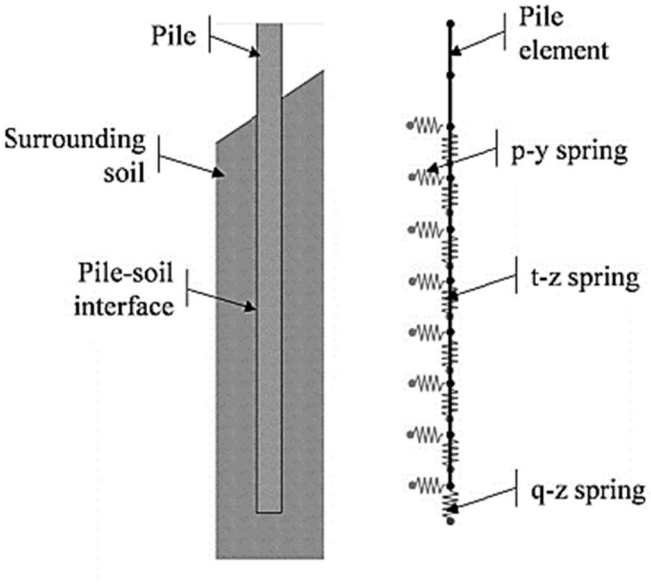

Figure 2-10 Schematic of soil springs.

- **p-y Springs**

A series of nonlinear springs (one spring/m) were assigned along the embedded length of piles during analysis. For p-y springs, two different force-deformation responses can be modeled directly in OpenSees. The first one is the p-y curve fit for soft clay soils in which the nonlinear properties are calculated from equations developed by Matlock (1970). The second response is fit for sand, the p-y curve of which can be built from tables available from (API 2002). In this project, the soil parameters used by Yang et. al (2012) were adopted. In their research, the behavior of stiff clay soils was assumed to be similar to that of soft clay, and "Pysimple" material was used to

model stiff clay. For soft clay soils in the presence of free water and static loading, the p-y can be derived based on the equations below (Figure 2-13 (a)) (Reese and Van Impe 2010):

$$\boldsymbol{P = \frac{P_{ult}}{2}\left(\frac{y}{y_{50}}\right)^{\frac{1}{3}}} \quad \text{(Eq. 2-1)}$$

$$\boldsymbol{y_{50} = 2.5\varepsilon_{50}b} \quad \text{(Eq. 2-2)}$$

where P_{ult} is the ultimate resistance of soil (Eq. 2-3); y_{50} is the lateral displacement when half of the ultimate soil resistance is reached; ε_{50} is the strain at the displacement of y_{50}; and b is pile's diameter.

$$\boldsymbol{P_{ult} = min\left(\left[3 + \frac{\gamma'}{c_u}z + \frac{J}{b}z\right]c_u b\,, 9c_u b\right)} \quad \text{(Eq. 2-3)}$$

where $\gamma'$is the average effective unit weight of soil; z is the depth of spring; c_u is the average undrained shear strength of the soil; and J was determined experimentally to be 0.5 for soft clay and 0.25 for medium clay (Matlock (1970)).

For the cyclic loading, the p-y curve is the same as of static loading for values of P less than $0.72P_{ult}$. The depth of z_r can be found in Equation 2-4:

$$\boldsymbol{z_r = \frac{6c_u b}{\gamma' b + Jc_u}} \quad \text{(Eq. 2-4)}$$

The value of z_r should be calculated for the desired depth of each spring. If the depth of spring is greater than z_r, then P is equal to $0.72P_{ult}$ for all values of y greater than $3y_{50}$, and if not, the value of P decreases from $0.72P_{ult}$ at $y = 3y_{50}$ to the $0.72P_{ult}(z/z_r)$ at $y = 15y_{50}$ (Figure 2-13 (b)).

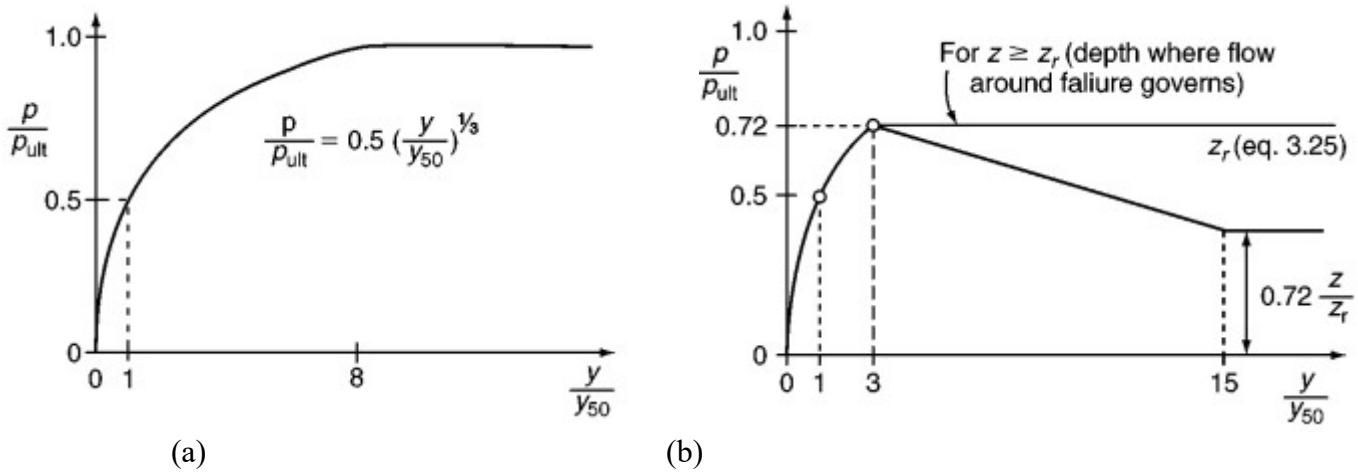

(a) (b)

Figure 2-11 p-y curves for soft clay in the presence of free water: (a) static loading; (b) cyclic loading. (Reese and Van Impe 2010)

Based on API (2002), the ultimate lateral bearing capacity for sand is the smaller values of P_{us} and P_{ud} (Eq. 2-5 to 2-7).

$$\boldsymbol{P_{us} = (C_1 H + C_2 b)\gamma' z} \quad \text{(Eq. 2-5)}$$

$$\boldsymbol{P_{ud} = C_3 b \gamma' z} \quad \text{(Eq. 2-6)}$$

$$\boldsymbol{P_{ult} = \min(P_{ud}, P_{us})} \quad \text{(Eq. 2-7)}$$

Values of C_1, C_2, and C_3 can be determined from Figure 6.8.6-1 of API (2002), using internal friction angle, ϕ'. The lateral load-displacement (p-y) relationship for sand can be derived from Eq. 2-8:

$$\boldsymbol{P = A.P_{ult}.\tanh\left[\frac{k.z}{A.P_{ult}}.\gamma'\right]} \quad \text{(Eq. 2-8)}$$

where A is a factor to take into account the effect of type of loading, whether static or cyclic. Hence, A is 0.9 for cyclic loading and is $(3 - 0.8z/b) \geq 0.9$ for static loading. The parameter k is the initial modulus of subgrade reaction which can be determined from Figure 6.8.7-1 of API (2002). In Table 2-5, the parameters used to model p-y springs for the bedrock layer are presented.

Table 2-5 Soil parameters for the rock fill. (Yang et al. 2012)

Piles	Z_t (1)(m)	Z_b (1) (m)	$Pult_t$ (kN / m)	$Pult_b$ (kN / m)	$y50_t$ (m)	$y50_b$ (m)
G, H	−1.2954	−11.2954	70.14	1402.75	0.00508	0.00178
F	−2.4384	−10.4384	43.84	1052.06	0.00254	0.00864
E	−6.0960	−10.0960	43.84	87.67	0.00254	0.00635

(1) Z_t and Z_b are the elevation at the top and bottom of each layer, respectively.

- **q-z Springs**

In addition to p-y springs, two types of vertical springs are needed, soil springs to simulate the nonlinear behavior of vertical response of soil, and pile tip bearing. The end bearing or tip-load capacity can be determined from Article 6.7.3 of API (2002) as shown in Figure 2-12. Y50 is the displacement relative to 50% of q_{ult} in monotonic loading. Based on API, a tip displacement of around 10% of the pile diameter may be required for full mobilization of tip strength for both sand and clay soils. So, a Y50 equal to 1.3% of pile diameter was used in this study. The detailed calculation of ultimate strengths can be found in Appendix A. For modeling of q-z spring, the mentioned load-deformation behavior is defined by implementing "*ElasticMultiLinear*" material available in the OpenSees library. The behavior only applies to compression load bearing. A rigid bearing was used for pile bearing on the rock in this project (Kim and Mission 2011).

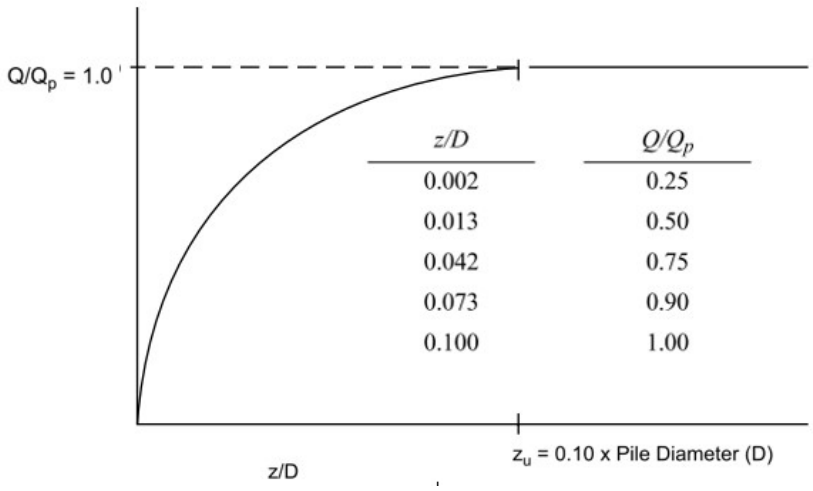

Figure 2-12 Pile tip load-displacement (q-z) curve. (API 2002)

- **t-z Springs**

The t-z springs in OpenSees take into account the friction between soil and pile. There are two models available in OpenSees which were proposed by Reese and O'Neill (1987), and Mosher (1984), respectively, to develop response curves for different soil conditions. However, the curves presented in Figure 2-13 are recommended by API in the case of the absence of any definitive criteria. In this figure, t is mobilized soil pile adhesion, and t_{max} is maximum soil pile adhesion or unit skin friction capacity. The API method was used to represent the force-displacement behavior of t-z springs.

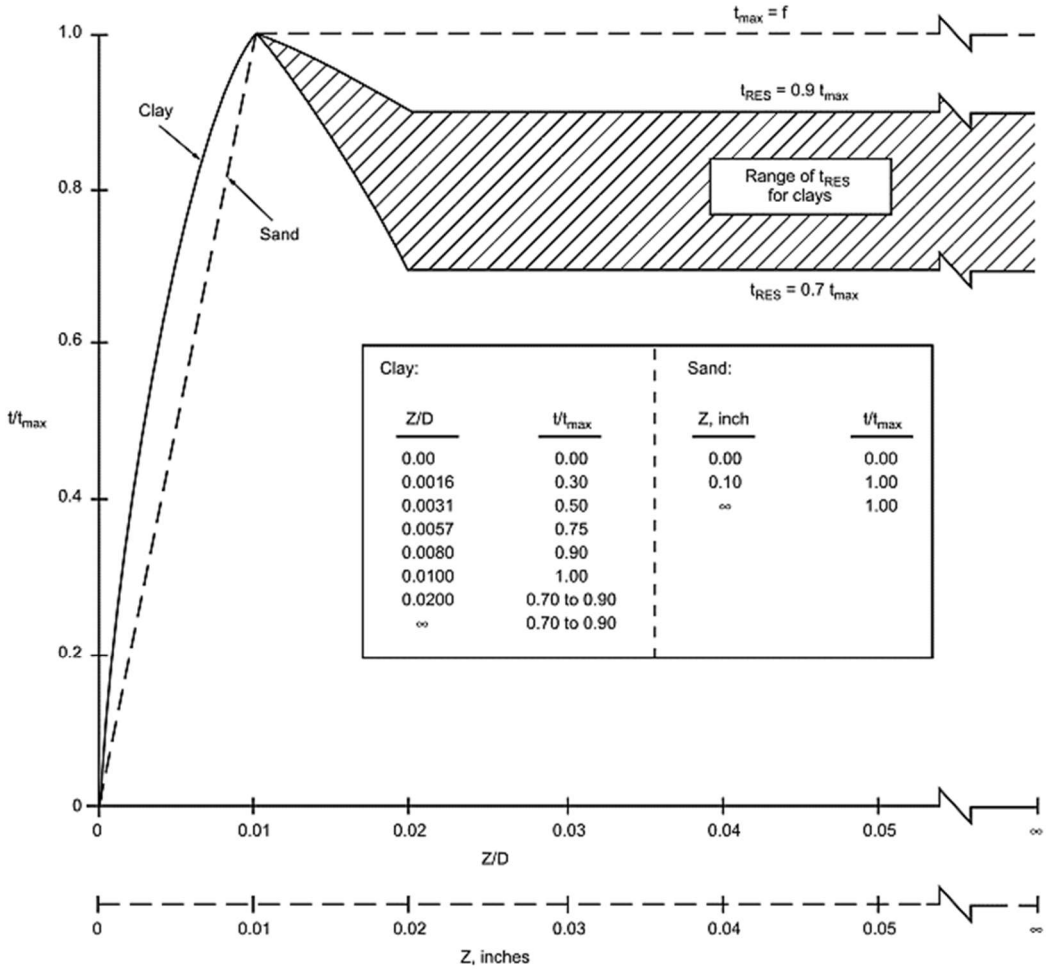

Figure 2-13 Typical axial pile load-displacement (t-z) Curves. (API 2002)

2.4 Damage States

To develop fragility curves, it is necessary to define the damage levels and damage criteria. These criteria can be derived based on actual damage data collected from field surveys in past earthquakes, experimental results, numerical simulation, or engineering judgment from experienced experts. Once the damage levels are defined, associated engineering demand parameters (EDPs) (damage criteria) can be specified for each level of damages. The EDPs for structural elements are usually displacement-based. By comparing the seismic response of structures with the damage criteria, the damage level of the structures can be determined.

In this research, strain limits provided by PIANC (2001) were employed to evaluate the risk of damage to the wharves under seismic load. Three different performance levels were introduced: serviceable, repairable damage, and severe damage (PIANC 2001).

2.4.1 PIANC Damage States

The working Group 34 of the Permanent International Association Navigation Congresses (PIANC) has proposed a set of damage states for typical port structures, including pile-supported wharves (PIANC 2001). The levels of damage are specified according to the needs of the port facilities and owners. They were defined based on the acceptable level of structural and operational damage given in Table 2-6. The specifications of the types of damage provided by PIANC were established based on the serviceability and structural damage levels of ports such as the safe operation of vehicles, interruption in berthing and mooring, displacements, and tilting concerning landside level, etc.

Table 2-6 Acceptable levels of damage in performance-based design [(1)] (PIANC 2001)

Level of damage	Structural	Operational
Degree I: Serviceable	Minor or no damage	Little or no loss of serviceability
Degree II: Repairable Damage	Controlled damage[(2)]	Short-term loss of serviceability[(3)]
Degree III: Severe Damage	Extensive damage in near collapse	Long-term or serviceability

(1) Protection of human life and property functions as an emergency base for transportation, and protection from spilling hazardous materials, if applicable, should be considered in defining the damage criteria in addition to those shown in this table.
(2) With limited inelastic response and/or residual deformation.
(3) Structure out of service for short to moderate time for repairs.

PIANC (2001) provides the strain limits for materials of pile sections for the first two damage states, serviceability, and damage control, as shown in Table 2-7. Also, It is assumed that the severe damage occurs when the materials of the section reach the strain limit of 2/3 of their ultimate strains, which is the strain corresponding to the maximum stress on the stress-strain curve (Shafieezadeh 2011).

Table 2-7 Strain limits for constitutive materials of prestressed concrete piles (PIANC 2001)

	Limit State		
	Serviceabille DS1	Repairable Damage DS2	Severe Damage DS3
Cover Concrete extreme fiber compression strain	0.004	0.008	-
Core concrete extreme fiber compression strain	-	-	$2/3\varepsilon_{cu}$ [(1)]
Reinforcing steel tension strain	0.01	0.05	$2/3\varepsilon_{su}$ [(1)]
Pre-stressing strand incremental strain	0.005	0.015	$2/3\varepsilon_{pu}$ [(1)]

(1) ε_{cu} is concrete's ultimate compressive strain.
(2) ε_{su} is steel dowel's ultimate compressive strain.
(3) ε_{pu} is prestressing strand's ultimate compressive strain.

Chapter 3: Ground Motion Selection

The seismicity of south-western British Columbia is affected mainly by the subduction of the oceanic Juan de Fuca plate beneath the North American continental plate occurring about 100 km west of Southern Vancouver Island (Figure 3-1). This geological situation may lead to three types of earthquakes that occurred on the west coast of British Columbia, i.e., the Cascadia interface, in-slab, and shallow crustal earthquakes. Interface earthquakes occur right at the interface between Juan de Fuca and North America plates. In-slab earthquakes have been recorded at a depth greater than 50 km, as deep as the Juan de Fuca plate, and shallow crustal earthquakes usually happen at a depth not greater than 20 km in the continental North America plate.

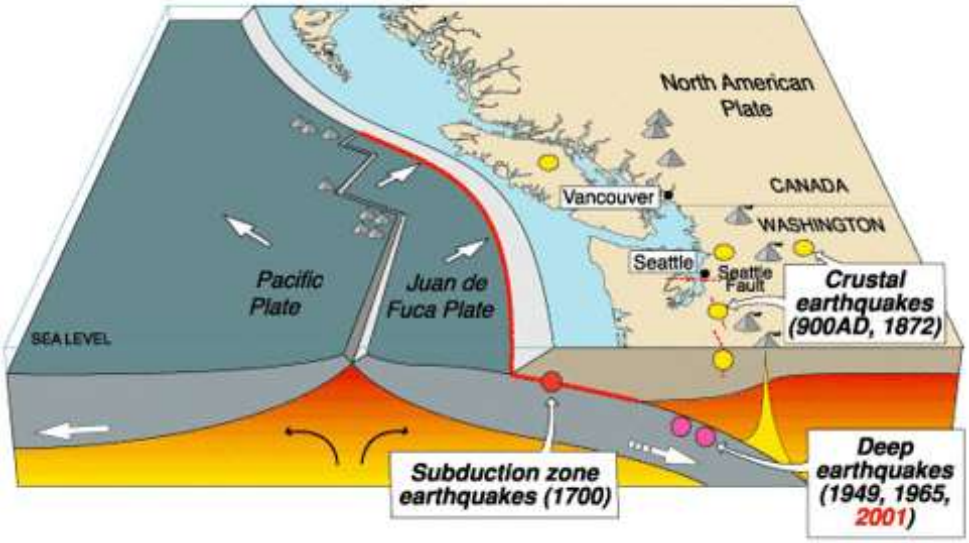

Figure 3-1 Cascadia subduction zone (USGS)

The pile-supported wharves usually belong to short-period structures (T = 0.26 s in this project), which can exhibit different seismic behavior during different types of ground motions. Thus, it is crucial to consider all sources of hazards for seismic risk assessment of port structures located in the Cascadia Subduction Zone. Figure 3-2 shows the deaggregated hazards for Vancouver. It can be seen that the in-slab earthquakes have the largest contribution to the hazard for short period structures (0.2s and 0.5s) in Vancouver. This is due to the combination effect of relatively higher magnitude, shorter distance to Vancouver, and higher frequency of occurrence of in-slab earthquakes, which makes this type of earthquake a significant hazard for short period structures in Vancouver. It is worth noting that although shallow crustal earthquakes have a considerable

effect on the performance of short-period structures, their contribution to the short-period hazard is low. This is due to the low magnitude and frequency of occurrence of this type of earthquakes (Rogers et al. 2015).

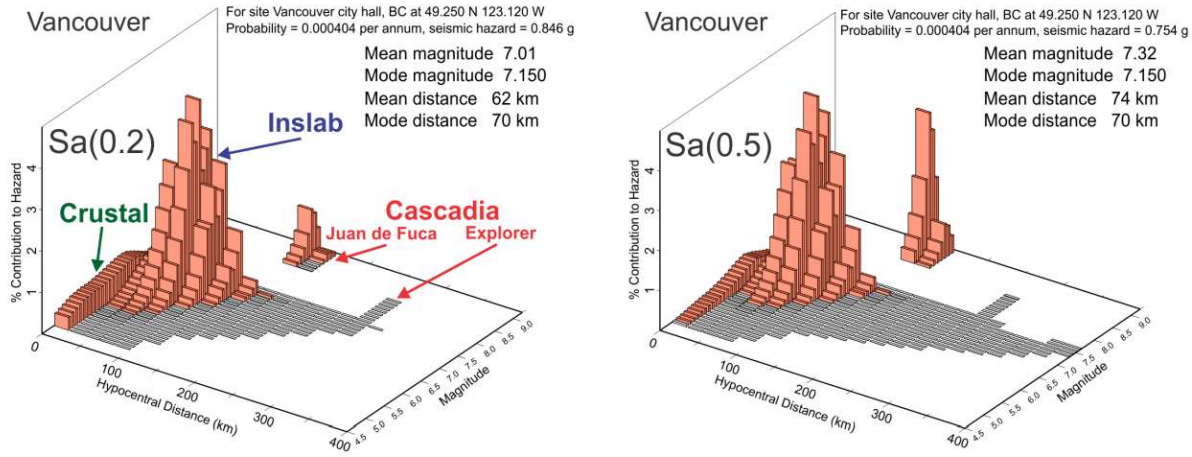

(a) (b)

Figure 3-2 Deaggregation of seismic hazard for Vancouver — contributions from three types of earthquake sources: a) Sa(0.2) structures; b) Sa(0.5) structures (Rogers et al. 2015)

Figure 3-3 shows the deaggregation of seismic hazard for short-period structures (T = 0.2 s), for two other cities located on Vancouver Island; Victoria and Nanaimo. It is perceptible that these two cities are similar to Vancouver in which the in-slab earthquakes have the dominant contribution to the short-period hazard. By comparing Figure 3-2 and Figure 3-3, it can be seen that the interface earthquakes in Victoria have a greater contribution in total seismic hazard in comparison with Vancouver and Nanaimo. This is due to the larger distance of Vancouver to the rupture area which causes more high-frequency motions (shorter periods) to be damped, which makes short-period structures less vulnerable to these events.

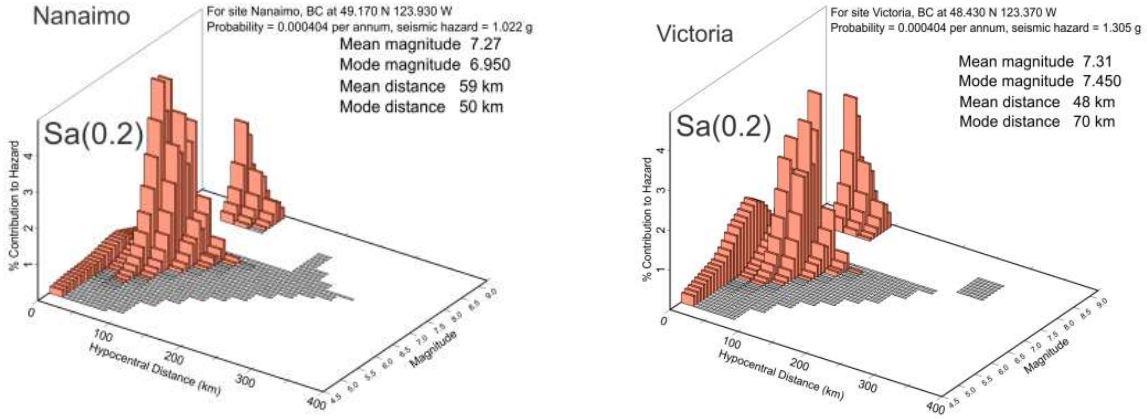

(a) (b)

Figure 3-3 Deaggregation of a seismic hazard: a) Nanaimo; b) Victoria. (Rogers et al. 2015)

Many parameters need to be considered while selecting ground motion records for a given site. According to Commentary J of the National Building Code of Canada (NBCC 2015), these parameters include magnitude, distance to the site, tectonic regime, local geotechnical conditions, and earthquake types, etc. The criteria considered in the selection of ground motions in this project are listed below:

- Site class C was chosen in this project for the design of the wharf structure, which refers to dense soils and matches with the soil properties cited from Yang et. al (2011). Therefore, the time-averaged shear wave velocity in the upper 30 m, Vs_{30}, is set to be between 360 m/sec and 760 m/sec (NBCC 2015).
- The range of distances to earthquake sources was selected to be representative of different locations of ports in British Columbia, especially in Vancouver. Thus, a rupture distance of 80-200 km for Cascadia interface events, and for in-slab and shallow crustal events, an epicentral distance of 30-100 km and 0-60 km, respectively, were selected in compliance with Pina et al. (2010).
- The moment magnitude of shallow crustal events was filtered to fall within the range of M_w 6.5-7.5 (Pina et al. 2010). Because of the lack of data recorded for interface events, a magnitude of M_w 8.2-9.0 was selected to be as close as possible to the Cascadia main event's expected magnitude (M_w = 9.0). For in-slab events, this range is between M_w 6.6 to 7.1.

- According to Appendix of Commentary J of NBCC (2015), no more than two records per station from the same events should be selected in the analysis. While there are not enough records for in-slab and interface ground motions, therefore, up to three records per station were selected for some events, especially for the Tohoku, Japan subduction event, which is the only available and closest event to the Cascadia magnitude of M_w 9.0.
- The records presented in Table 3-1 were downloaded from different sources. Shallow crustal earthquakes were downloaded from the PEER NGA West2 Ground Motion Database (PEER), which have already been processed and can be used directly for analysis. In-slab earthquake records were downloaded from USGS National Strong Motion Program (USGS), Japanese K-Net and KiK-Net Networks (KiK-Net); and Subduction interface earthquake records were downloaded from Center for Engineering Strong Motion Data (CESMD) and Japanese K-Net and KiK-Net Networks.
- The records downloaded from the Japanese database require baseline correction and filtering before they can be used for analyses. The filter used in this study is BUTTERWORTH-Bandpass-4^{th}-order filter (Pina et al. 2010), which was developed with MATLAB software. The default upper-bound and lower-bound frequencies used for filtering were 25 Hz and 0.10 Hz (Pina et. Al 2010), respectively. However, for some records, the filter ranges were refined to eliminate the noise in the recordings. Also, it is crucial that the mentioned frequency range encompasses the period range provided by NBCC 2015. The period range recommended by NBCC 2015 Commentary J is from 0.15T to 2T, where T is the fundamental period of the structure (0.26 sec).
- Also in the case of shallow crustal events, two different groups were selected, pulse-like and non-pulse-like, to investigate the effect of possible hidden faults under the Vancouver area on the response of the wharf. Records recorded at closer distances contain a velocity pulse in their time series.
- There were eleven ground motions selected for each type of earthquake and each motion includes two components.

Table 3-1 Selected ground motions list

			Earthquake	Date	Station	Faulting	M_w
Shallow Crustal	1	Pulse-Like	Loma Prieta	1989	Gilroy Array #3	Reverse/oblique	6.93
	2		Chi-Chi	1999	TCU036	Reverse/oblique	7.62
	3		Niigata	2004	NIG021	Reverse	6.63
	4		Chuetsu-oki	2007	Joetsu Kakizakiku Kakizaki	Reverse	6.8
	5		Northridge-01	1994	Pardee - SCE	Reverse	6.69
	6	No Pulse-Like	Loma Prieta	1989	Anderson Dam (L Abut)	Reverse/oblique	6.93
	7		Northridge-01	1994	Glendale - Las Palmas	Reverse	6.69
	8		Lytle Creek	1970	Colton - So Cal Edison	Reverse/oblique	5.33
	9		San Fernando	1971	LA - Hollywood Stor FF	Reverse	6.61
	10		Cape Mendocino	1992	Ferndale Fire Station	Reverse	7.01
	11		Coalinga-01	1983	Parkfield - Vineyard Cany 1E	Reverse	6.36
In-slab	12		Nisqually, WA	2001	Tacoma; VA Hospital; Bldg 81;		6.8
	13		Nisqually, WA	2001	Seattle; Ship Canal Bridge		6.8
	14		Nisqually, WA	2001	Wynoochee Dam; upper gallery		6.8
	15		Geiyo, Japan	2001	Tohyu		6.7
	16		Geiyo, Japan	2001	Mihara		6.7
	17		Geiyo, Japan	2001	Mikawa		6.7
	18		Guerrero, Mexico	1994	Zihuatanejo (AZIH)		6.6
	19		Michoacan, Mexico	1997	Villita (VILE)		7.1
	20		Michoacan, Mexico	1997	La Union		7.1
	21		Michoacan, Mexico	1997	Caleta De Campos		7.1
	22		Guerrero, Mexico	1994	El Balcon		6.6
Interface	23		Tohoku, Japan	2011	Oshika MYG011		9
	24		Tohoku, Japan	2011	Dattoh IWT009		9
	25		Tohoku, Japan	2011	Tahakata YMTH06		9
	26		Tokachi-oki, Japan	2003	HKD092 IKEDA		8.3
	27		Tokachi-oki, Japan	2003	HKD100 HIROO		8.3
	28		Maule, Chile	2010	Concepcion		8.8
	29		Maule, Chile	2010	Curico		8.8
	30		Maule, Chile	2010	Angol		8.8
	31		Coquimbo, Chile	2015	San Esteban		8.3
	32		Coquimbo, Chile	2015	El Pedregal		8.3
	33		Iquique, Chile	2014	Chusmiza		8.2

Chapter 4: Seismic Performance of Port Structures

4.1 Incremental Dynamic Analysis

In the nonlinear incremental dynamic analysis (IDA), two parameters need to be determined. The first one is a proper intensity measure (IM) of ground motions, and the second one is an appropriate engineering demand parameter (EDP) representing the performance of structures. In the IDA approach, Amirabadi et al (2012) suggested using 5% damped spectral acceleration, S_a (T_1, 5%), as IM to scale the ground motion records where T_1 is the fundamental period of structures from the modal analysis. For EDP, PIANC recommended using peak response of the piles, like the strain of materials, as the proper parameter to trace the development of damage.

In this project, each ground motion was scaled linearly (Chiou et. al 2011) with an interval of 0.15g based on the spectral acceleration of records, S_a, at the fundamental period (0.26s) of the pile-supported wharf structure. The wharf's response, the strain of concrete and steel materials, was recorded under each shaking level to determine the maximum response and the damage levels. The process was repeated until the desired structural limit state presented in Table 2-7 was reached. In the following sections, the results and observations based on the IDA analyses are discussed.

4.2 Failure Mode

The critical damage tends to start at the top of the shortest piers (H and G in Figure 4-1) of the wharf structure analyzed in this study, and the short-period response appears to have the most influence on the damage. Figure 4-1 shows, schematically, the general behavior of the pile-supported wharf subjected to seismic events. The wharf analyzed in this project has a considerably stiff deck that leads to a pretty uniform lateral displacement to all piles. As a result, short piles with a relatively larger lateral stiffness experienced higher seismic force and pile-deck rotation. The modeling analysis results show that cracks and minor damage usually initiated at the top of the shortest piles G and H. As the seismic load increases, cracks were developed on piles just below the soil surface. At the meantime, damage at the top head of the shortest pile was further developed, and minor damage started to occur at the top of the other piles located towards seaward.

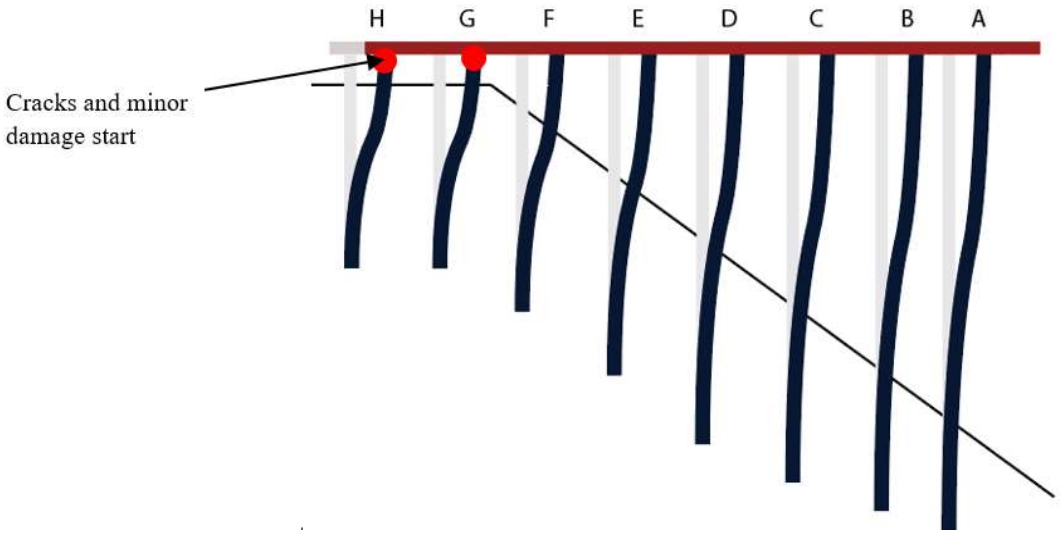

Figure 4-1 Damage initiation in the pile-supported wharf

4.3 Pulse-like and No-Pulse-like Crustal Ground Motions Effect

Pulse-like ground motions are often caused by forward-directivity effects and might cause severe damage to structures with a certain period that is close to the period of pulse. As an example, two records were selected from Northridge-01 1994 event, one with a pule-like component which was recorded at Pardee - SCE station, and the other without pulse which was recorded at Glendale - Las Palmas station. Figure 4-2 shows the time-history displacement response of the pile-supported deck at S_a = 2.0g intensity level. As can be seen, the response of the wharf is greater in pulse-like ground motion. To explore deeper, Figure 4-3 depicts the reason behind this result. It is perceptible that the pulse increases the seismic demand in a wider range of periods, which encompasses the elongated period of the wharf as damage propagated. As highlighted in Figure 4-3, any small increase in the period from the elastic period range, 0.26s, the acceleration demand increases significantly. In Figure 4-4, the large velocity component is recognizable in pseudo velocity spectrums of records.

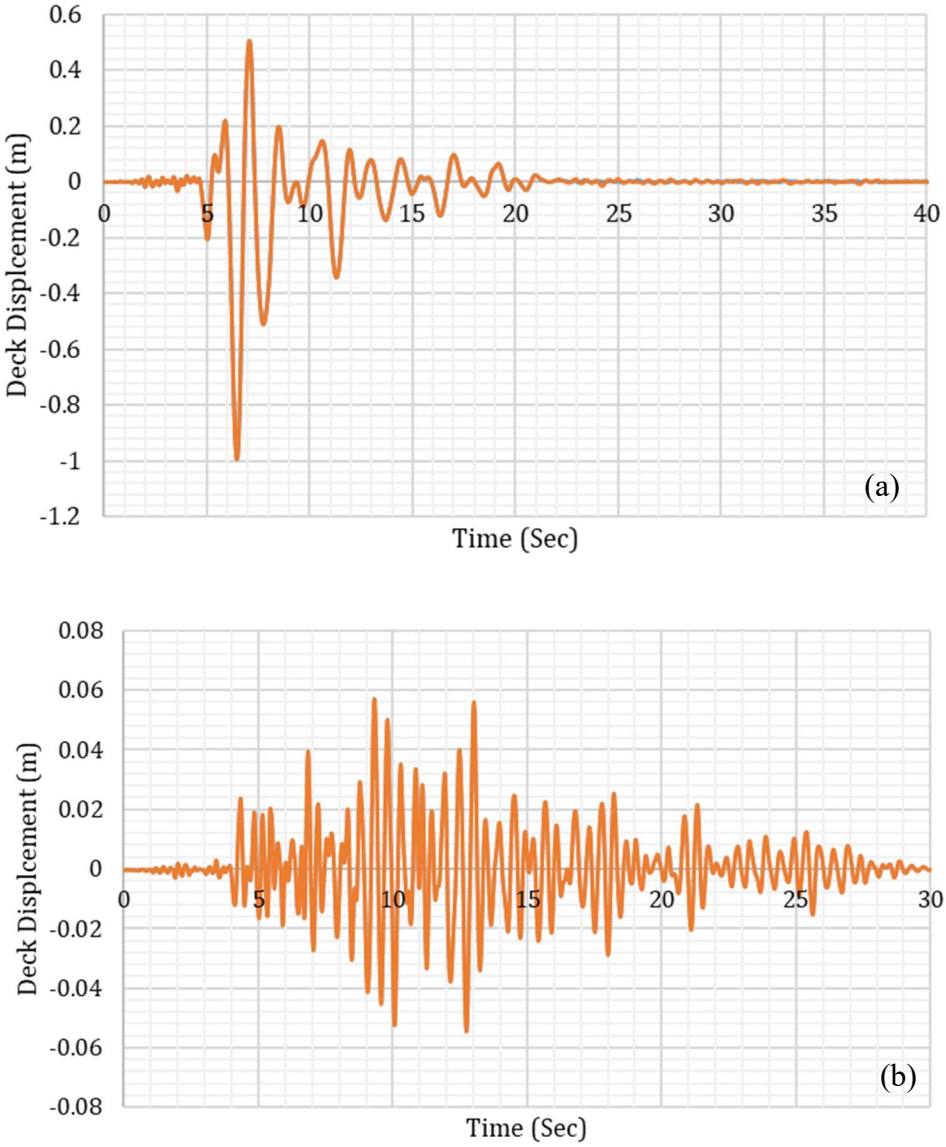

Figure 4-2 Deck horizontal displacement of wharf at S_a=2.0g ground motion intensity: a) Northridge-01(1994)- Glendale - Las Palmas St., component #2;b) Northridge-01 (1994)- Pardee SCE St., component #2

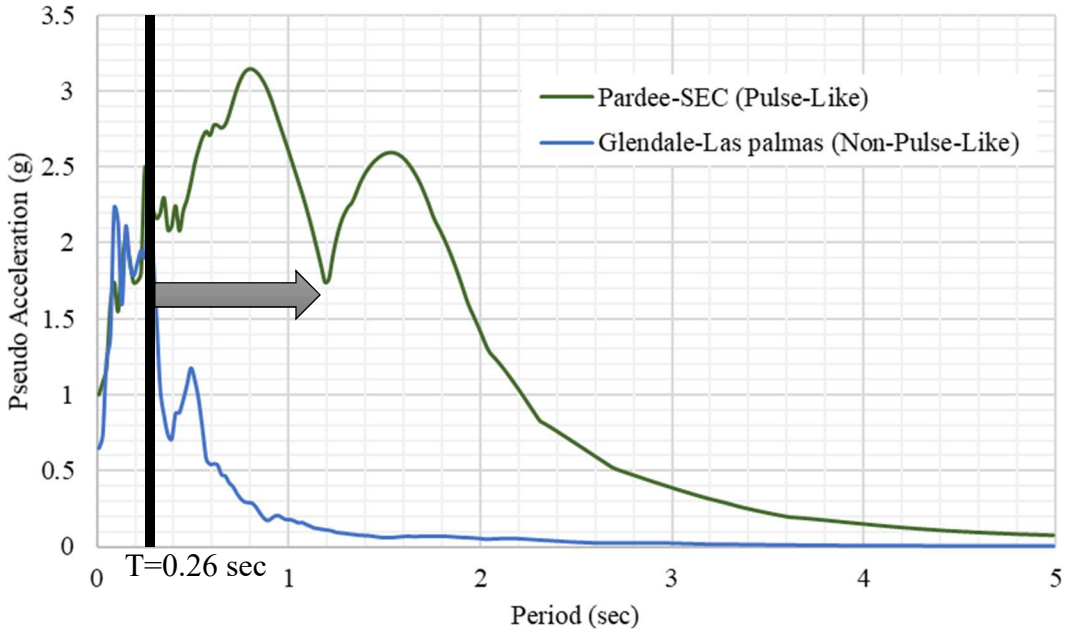

Figure 4-3 Pseudo spectral acceleration of Northridge-01 records (Scaled to S_a = 2.0g)

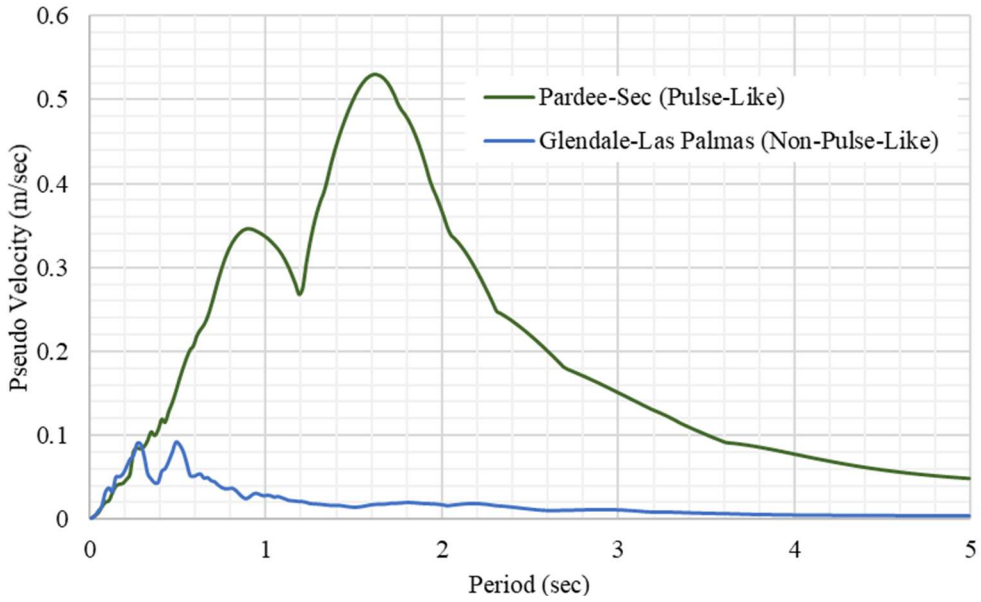

Figure 4-4 Pseudo spectral velocity of Northridge-01 records (Scaled to S_a = 2.0g)

4.4 IDA Curves under Different Earthquakes

Figure 4-5 shows the median IDA curves for three different types of ground motions. It is evident that shallow crustal events affect the performance of wharf structure most within the three types of earthquakes. This is mostly due to their frequency content, and the pulse-like ground motion effect as discussed in the previous section.

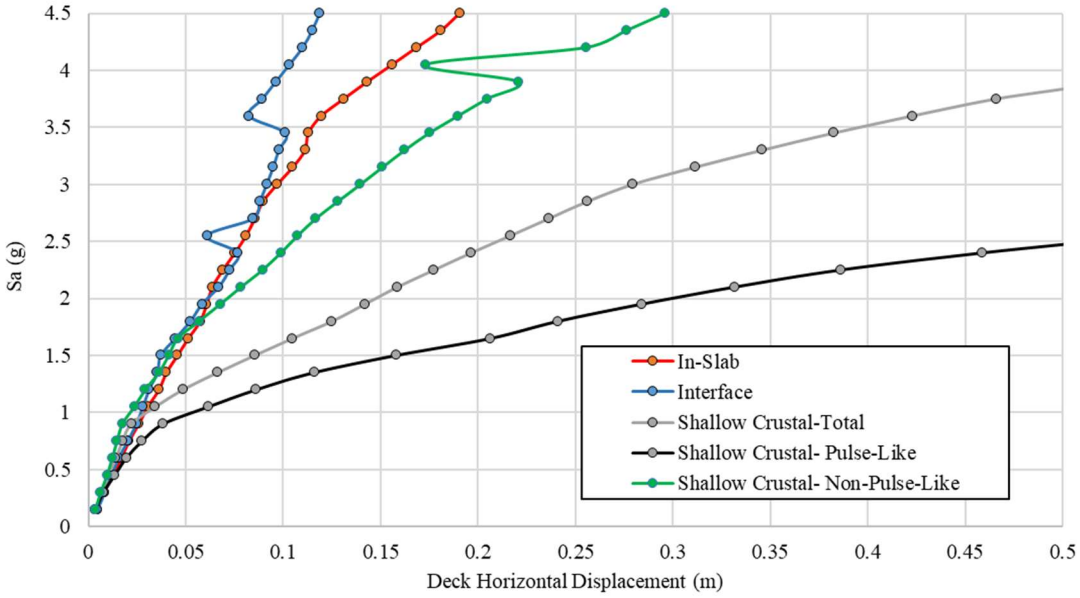

Figure 4-5 Median IDA curves for three types of ground motions

Also, as was anticipated, pulse-like shallow crustal events resulted in higher seismic demand, and subsequently, the wharf structure experienced damage at lower hazard levels under shallow crustal earthquakes.

4.5 Fragility Analysis

In this study, the probability of exceeding a damage state for a given hazard level is calculated for the three types of earthquakes (Table 2-7). For each damage state, DS_i, a separate fragility curve was developed, demonstrating the probability of the wharf exceeding the damage state DS_i at a specific seismic level. The limit states associated with recorded responses were assumed to be lognormally distributed, and the probability of damage is calculated based on Eq 4-1 to Eq 4-3.

$$\boldsymbol{P[EDP > DS_i | \, IM = S_a] = 1 - \Phi\left[\frac{\ln(x_i) - \alpha}{\beta}\right]} \qquad \text{(Eq. 4-1)}$$

$$\alpha = \ln \mu - \frac{1}{2}\beta^2 \qquad \text{(Eq. 4-2)}$$

$$\beta = \sqrt{\ln\left[1 + \left(\frac{\sigma}{\mu}\right)^2\right]} \qquad \text{(Eq. 4-3)}$$

where EDP is the engineering demand parameter, which is the strain of steel and concrete; IM is the intensity of ground motion represented by the spectral acceleration at the fundamental period of the structure S_a; Φ is the standard normal cumulative distribution function; x_i is the spectral acceleration of each ground motion that causes DS_i, μ is the median and σ is the standard deviation of the sample population. Figure 4-6 shows the fragility curves for three types of ground motions under three different damage levels (minimal damage DS1, controlled and repairable damage DS2, and life safety protection DS3). Table 4-1 summarizes the median spectral accelerations of occurrence of each damage state. The median values have a probability of occurrence of 50%.

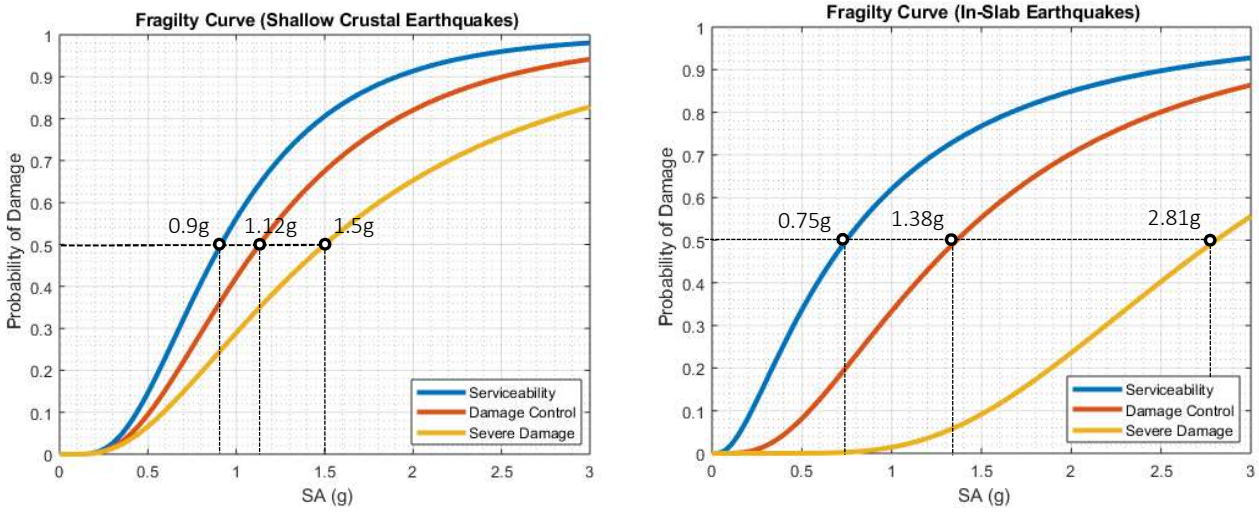

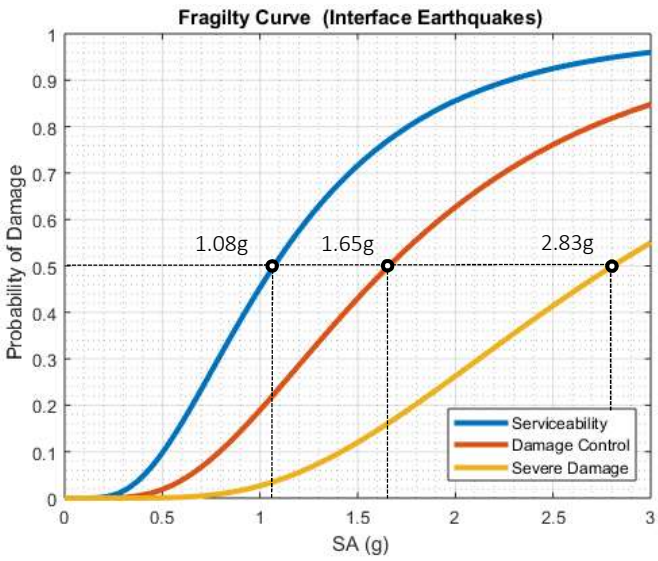

Figure 4-6 Fragility curve for a) Shallow crustal; b) In-slab; and c) Interface earthquakes

Table 4-1 Median Sa with probability of occurrence of 50% for each damage state

Ground motion Type	Serviceable	Repairable Damage	Severe Damage
Shallow Crustal	0.90g	1.15g	1.50g
In-Slab	0.75g	1.38g	2.81g
Interface	1.08g	1.65g	2.83g

To interpret the result, the frequency content of selected ground motions (all scaled to a PGA of 9.81 m/sec^2) was analyzed in terms of Fourier amplitude and pseudo-spectral acceleration, as shown in Figure 4-7 and Figure 4-8, respectively. It can be seen that in in-slab earthquakes, in comparison with the interface and shallow crustal earthquakes, the contribution of high frequency (low period) motions (more than 1 Hz) is higher which led to a higher risk of serviceable damage (DS1) occurrence (smaller IM of 0.75g compared to 0.90g and 1.08g in Table 4-1). Figure 4-9 shows the Fourier transform of the time-history response of the wharf structure under Loma Prieta 1989 Gilroy Array #3 record (shallow crustal records #1 in Table 5) at different seismic levels, from Sa = 0.15g to Sa = 4.5g. Also per Figure 4-9, it can be seen that higher seismic loads lead to extensive damage which elongates the dominant period of vibration. Therefore, as the period of vibration moves to the low-frequency region (longer period, more than 1.0 sec), it falls within the zone which is more vulnerable to crustal earthquakes. Thus, the IM causes a 50% probability of

damage to the port structure under shallow crustal events is smaller than that of the other two types of ground motions (1.50g compared to 2.81g and 2.83g in Table 4-1). It indicates that under shallow crustal earthquakes, the wharf structure reaches faster to DS3.

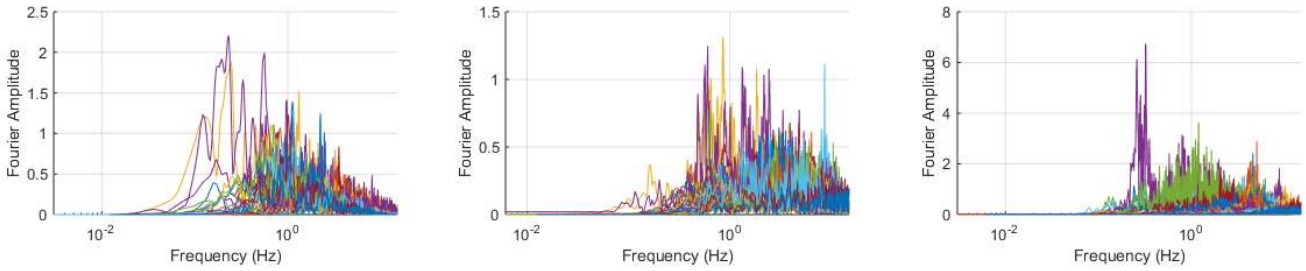

(a) (b) (c)

Figure 4-7 Furrier spectrum of ground motions: a) shallow crustal; b) in-slab; and c) interface.

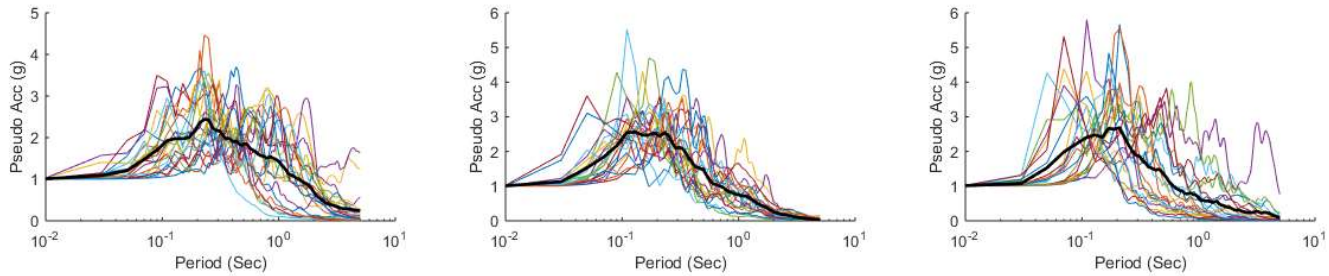

(a) (b) (c)

Figure 4-8 Spectral acceleration of ground motions: a) shallow crustal; b) in-slab, and c) interface.

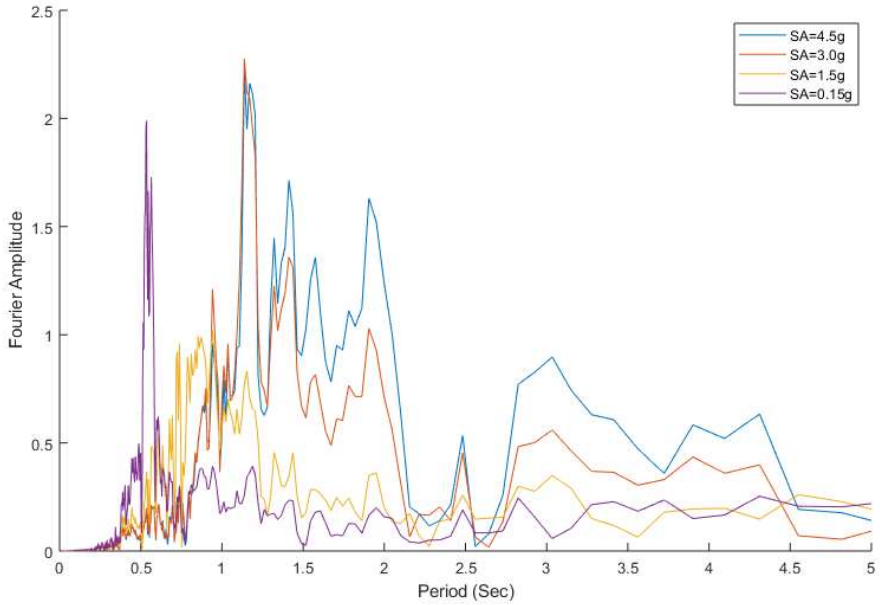

Figure 4-9 Change in the dominant period of vibration under different seismic intensity (Loma Prieta- Gilroy Array #3

It worth noting that despite the higher risk of damage levels 2 and 3 (DS2 and DS 3) due to the shallow crustal earthquakes compared to in-slab and interface events, based on the deaggregation of seismic hazard for Vancouver (Rogers et al. 2015), their contribution to the total seismic hazard is less than the other two types of ground motions. Hence, it is required to calculate the risk of damage based on Vancouver's seismic hazard values of 2% probability of exceedance in 50 years. The values listed in Table 4-2 are the aggregated seismic hazard values for short period hazard (0.26 sec) in Vancouver. Using these values, the probability of damage has been calculated for each hazard level.

Table 4-2 Probabilistic seismic hazard values Sa (0.26 sec) (Natural Resources Canada)

City	2% exceedance in 50 years
Vancouver	0.84g

The probabilities of damage at different seismic damage levels for wharves located in Vancouver have been presented in Figure 4-10. As shown, the results indicate that the shallow crustal events have a higher probability of causing controllable and severe damage. Also, it can be interpreted that in case of an event with 2475 years return period, the risk of controllable damage and severe damage under in-slab and interface ground motions for a wharf located in Vancouver is acceptable (less than 10%). It worth noting that, in-slab events are more important in case of minimal damage since the contribution of high-frequency motions in these events are higher.

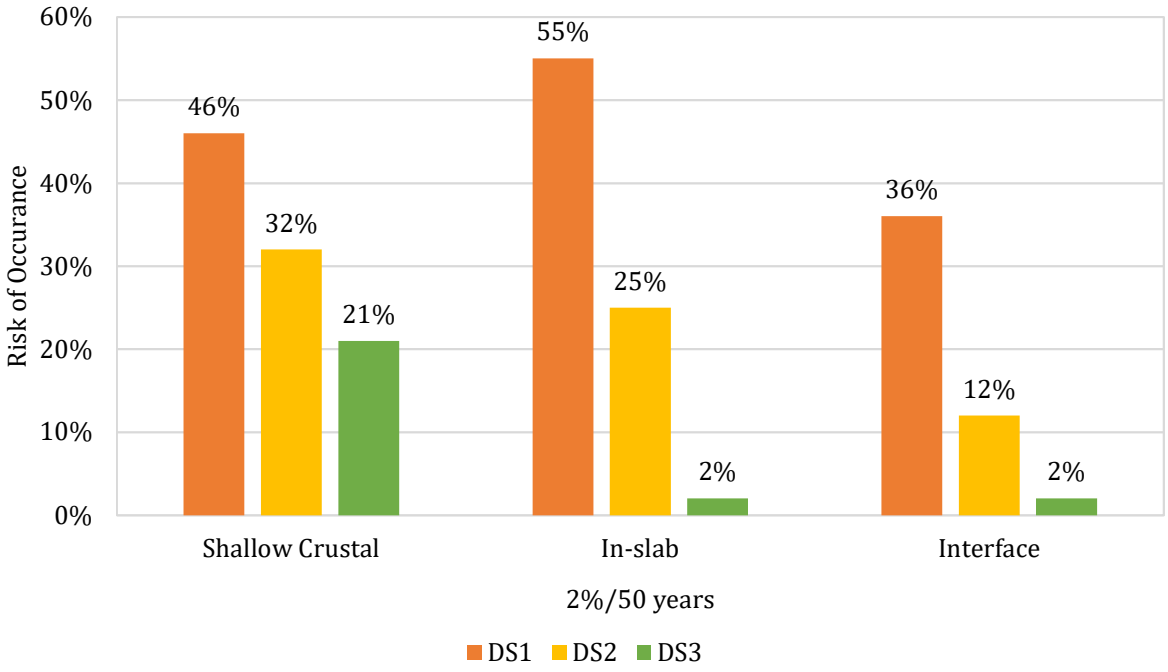

Figure 4-10 Probability of damage at different seismic levels

In regards to the hazard from Cascadia interface earthquakes, at the 2% probability of exceedance in 50 years hazard level, the risk of minimal damage is fairly high (36%); while controllable damage for a wharf located in Vancouver is less likely to happen (12%). In general, the effect of the Cascadia interface earthquake is not crucial for wharves (short-period structures) located in Vancouver (or lower mainland). In Figure 4-10, the risk values were calculated based on equal hazard levels, which is useful in terms of comparing the effect of earthquake types. But actually, the hazards coming from a different source of earthquakes in the Cascadia Subduction Zone are different. Figure 4-11 shows the deaggregated spectra of each type of earthquake for

Vancouver, Site Class C, with a probability of exceedance of 2% in 50 years (2475-year return period) (Bebamzadeh et al. 2015).

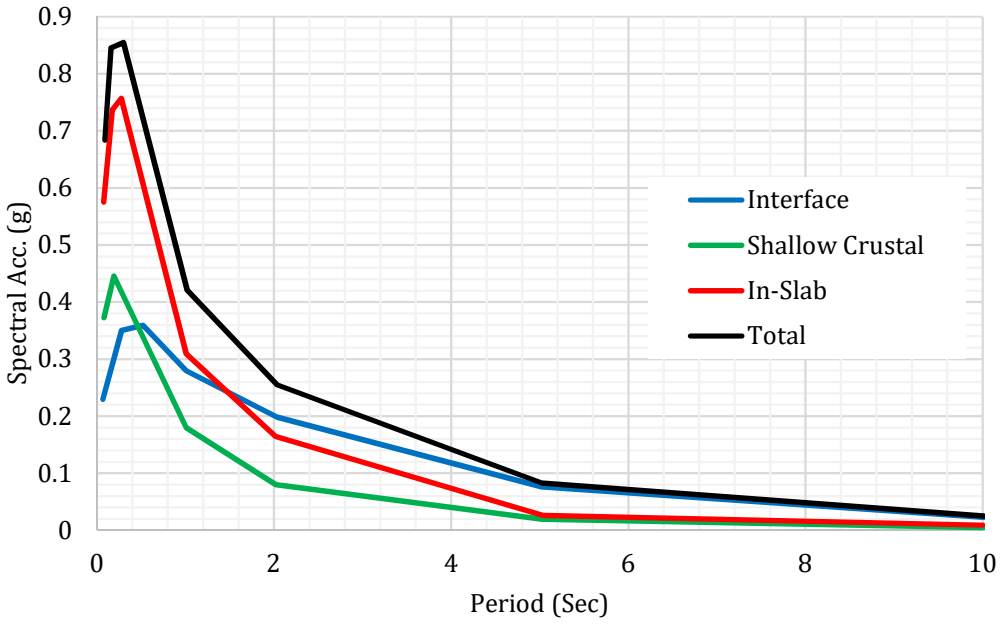

Figure 4-11 Deaggregated spectral accelerations of each type of earthquakes, 5% damped, Site class C, Vancouver (Bebamzadeh et al. 2015)

Table 4-3 Probabilistic seismic hazard values Sa (0.26 sec) based on Figure 4-11

City	Shallow Crustal (2475 years return period)	In-Slab (2475 years return period)	Interface (2475 years return period)
Vancouver	0.40g	0.76g	0.37g

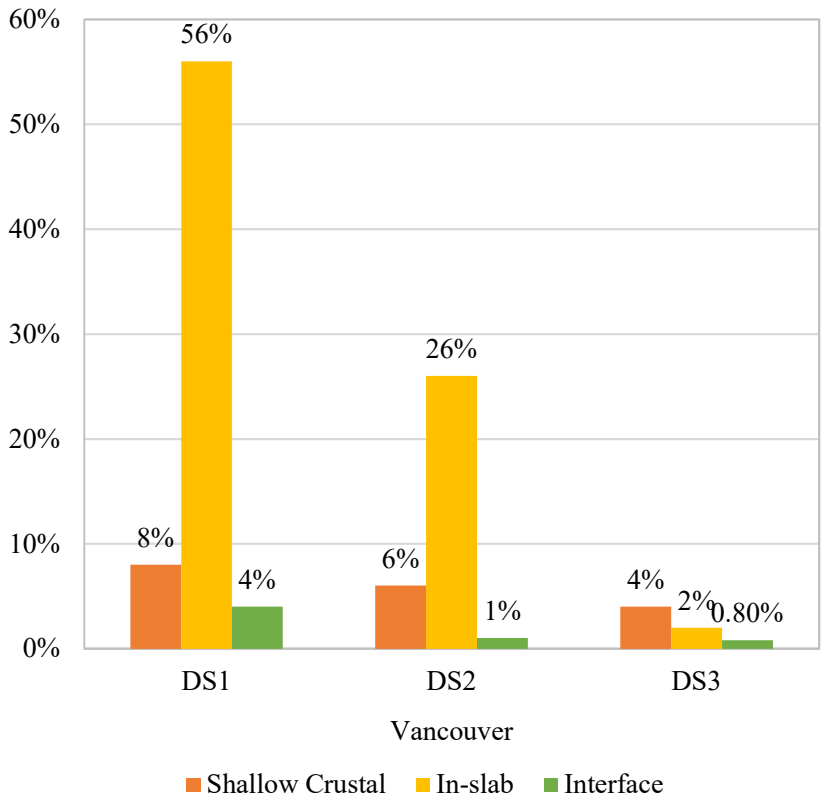

Figure 4-12 Probability of damage at different seismic levels based on deaggregated hazard

Figure 4-12, the risk of an in-slab earthquake is significant, and that is the dominant earthquake type for the period range of wharf structures in Vancouver. Meantime, shallow crustal events play an important role in reaching the damage state of DS3, as discussed earlier.

As shown in the results, the interface earthquake does not have a severe effect as it is presumed to have. This is due to the fact that the distance of selected interface earthquakes to the site (80-200 km) is far more than the other two types of earthquakes (0-60 km and 30-100 km for shallow crustal and in-slab, respectively), which makes the interface earthquakes less severe in terms of frequency content for short-period structures. The effect of rupture to site distance on the ground shaking at the site and its effect on wharves' seismic behavior is illustrated in Figure 4-14. Figure 4-14 shows the comparison of IDA curves of the pile-supported wharf under two ground motions recorded from the same earthquake (Maule, Chile 2010). They are Concepcion and Angol motions with a distance to the site of 82 km and 209 km respectively. Figure 4-13 shows, due to the damping of short period frequencies of ground motions in the larger distance, the wharf structure (a short-

period structure) exhibits less response at the same seismic intensity compared to that of a shorter distance site.

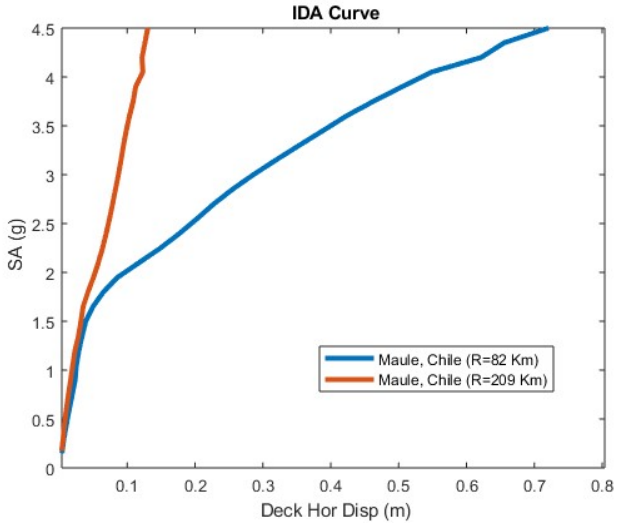

Figure 4-13 Comparison the effect of distance of hypocenter to site on seismic performance of the pile-supported wharf

Chapter 5 Conclusion

In this study, incremental nonlinear dynamic analyses were utilized to investigate the damage probability of a typical pile-supported wharf located in Vancouver, with a focus on three types of earthquakes that may occur in the Cascadia Subduction Zone. The wharf was assumed to be located on soil type C and was designed based on ASCE 61(2014). A two-dimensional nonlinear model of the wharf was developed using OpenSees software. The acceptable levels of damage (serviceable, repairable damage, and severe damage) were defined based on PIANC (2001) and the strain limit of materials corresponding to each damage level was determined. By applying lognormal distribution on IDA's results, three different sets of fragility curves for each type of earthquake were developed. The risk of occurrence of serviceability damage state, repairable damage, and severe damage were calculated based on aggregated and deaggregated response spectrums in Vancouver. Based on the results, it was found that:

- The damage initiation mostly concentrates at the top of piles, in the pile-deck connection zone. In this project, the damage was initiated at the top of the two shortest piles, G and H (Figure 2-1), which triggered the damage limit states.
- In this study, to evaluate the effect of pulse-like ground motions on the performance of wharves, and also to consider the existence of any hidden faults under the Metro Vancouver area, the pulse-like shallow crustal ground motions were considered as well. It was found that the pulse effect can increase the seismic demand and damage level. By developing the median IDA curve for both groups, Figure 4-5, it was observed, the pulse-like motions increase the probability of damage.
- Shallow crustal earthquakes can cause a higher probability of repairable and severe damage levels because of their frequency content. However, in-slab events are more important in case of minimal damage, since the contribution of the high-frequency motions in in-slab events is relatively higher.
- By utilizing the deaggregated hazard of Vancouver (NRCan), in-slab earthquakes imposing a higher risk for wharf structures in Vancouver.
- As shown in this thesis, interface earthquake, because of their relatively long distances to site, and therefore possess higher long-period components of shaking, has the lowest risk of damage on wharf structures among the three types of earthquakes analyzed, for wharves located on site

class C and in the lower mainland. Based on the analysis result of interface earthquakes, the distance from the rupture area can affect the frequency content of records. At larger distances, more high-frequency motions are damped and eventually, lead to a lower probability of failure of short-period structures.

5.1 Scope of the research

It is worth noting that the application of these results, especially fragility curves, is limited to the newly designed wharves based on ASCE 61 (2014) and the results may be sensitive to the specific ground motion records selected in the project. Also, the buckling of longer piles and the P-Delta effect were ignored in this project. Consideration of buckling may cause wharves more sensitive to long-period ground motions from subduction interface earthquakes. Besides that, the soil liquefaction effect on the seismic response of the wharf was excluded in nonlinear modeling. In this research, only horizontal components of earthquakes were considered. For future works, the effect of vertical components can be considered as well, especially for in-slab and pulse-like shallow crustal events.

The conclusions summarized in this project is only applicable for structures located at soil type C. The response of structures may differ if softer soil was selected, especially under interface events.

References

Amirabadi, R., Bargi, K., & Torkamani, H. H. (2012). Probabilistic Seismic Demand Models of PEER-PBEE framework for Pile and Deck Structures. International Journal of Civil and Structural Engineering, 2(3), 766.

American Petroleum Institute (2002). Recommended practice for planning, designing, and constructing fixed offshore platforms (Vol. 2).

American Society of Civil Engineers. (2014). Seismic Design of Piers and Wharves Standard ASCE/COPRI 61-14. Reston, VA.

American Society of Civil Engineers. (2016). Minimum Design Loads for Buildings and Other Structures (ASCE/SEI 7-16).

Municipal Affairs and Hausing (2018). British Colombia Building Code. BC, Canada.

Bebamzadeh, A., Fairhurst, M., Ventura, C. E., & Finn, W. L. (2015). "Selection of ground motions for the seismic risk assessment of british columbia school buildings for the proposed 2015 nbcc ground motions." Paper presented at the The 11th Canadaian Conference of Earthquake Engineering.

Boulanger, R. W., Curras, C. J., Kutter, B. L., Wilson, D. W., & Abghari, A. (1999). Seismic soil-pile-structure interaction experiments and analyses. Journal of geotechnical and geoenvironmental engineering, 125(9), 750-759.

Center for Engineering Strong Motion Data CESMD. Retrieved from http://www.strongmotioncenter.org.

Chiaramonte, M. M., Arduino, P., Lehman, D. E., & Roeder, C. W. (2013). "Seismic analyses of conventional and improved marginal wharves." Earthquake Engineering & Structural Dynamics 42(10): 1435-1450.

Chiou, J, Chi-Han C, Ho-Hsiung Y, and Shang-Yi H. (2011). "Developing fragility curves for a pile-supported wharf." Soil dynamics and earthquake engineering 31, no. 5-6: 830-840.

Applied Technology Council (1992). "ATC-24: Guidelines for seismic testing of components of steel structures."

Cowdell, S. R., Kendrick, W. S., & Acton, P. J. (2001) "Cruise Ship Terminal Expansion-Port of Vancouver, Canada." In Ports' 01: America's Ports: Gateway to the Global Economy, pp. 1-11.

Erdik, M. (2000). Report on 1999 Kocaeli and Düzce (Turkey) earthquakes, Boğaziçi Üniversitesi, Kandilli Rasathanesi ve Deprem Araştirma Enstitüsü.

Heidary-Torkamani, H., Bargi, K., & Amirabadi, R. (2014) "Seismic vulnerability assessment of pile-supported wharves using fragility curves." Structure and Infrastructure Engineering 10, no. 11: 1417-1431.

Jellin, A. R. (2008). Improved seismic connections for pile-wharf construction. (PhD diss), University of Washington.

Kayen, R. E., Mitchell, J. K., Seed, R. B., & Nishio, S. y. (1998). Soil liquefaction in the east bay during the earthquake. The Loma Prieta, California Earthquake of October 17, 1989-Liquefaction, US Geological Survey Professional Paper 1551-B, 61-86.

Kim, H.-J. and J. L. Mission (2011). "Probabilistic evaluation of economical factor of safety for the geotechnical design of pile axial load capacity." KSCE Journal of Civil Engineering 15(7): 1167.

Ko, Y. Y. and H.-H. Yang (2019). "Deriving seismic fragility curves for sheet-pile wharves using finite element analysis." Soil Dynamics and Earthquake Engineering 123: 265-277.

Ko, Y. Y., Yang, H. H., & Chen, C. H. (2010) "Seismic fragility analysis for sheet pile wharves—Case study of the Hualien harbor in Taiwan.". InFifth International Conference onRecent Advanced in Geotechnical Earthquake Engineeringand Soil Dynamics and Symposium in Honor of Professor I.M. Idriss, San Diego, CA, Paper No. 6.05a.

Torkamani, T. H., Bargi, K., and Amirabadi, R. (2013) "Fragility curves derivation for a pile-supported wharf.": Journal of Marine Engineering1(1): 1–10.

Lehman, D. E., Roeder, C., Stringer, S. J., & Jellin, A. (2013) "Seismic performance of improved pile-to-wharf deck connections." PCI journal 58, no. 3.

Na, U. J., Chaudhuri, S. R., & Shinozuka, M. (2009) "Performance evaluation of pile-supported wharf under seismic loading." In TCLEE 2009: Lifeline earthquake engineering in a multihazard environment, pp. 1-10.

Nakahara, T., Takahiro S., Ken O., and Masaaki M. (2000) "An experimental Study on the pier damaged by 1995 Hygoken-Nanbu earthquake." In Proc. 12 th World Conf. Earthq. Eng.

Natural Resource of Canada (2020). from https://earthquakescanada.nrcan.gc.ca/.

Pacific Earthquake Engineering Research Center PEER, (2020). http://ngawest2.berkeley.edu

PIANC. (2001). Seismic Design Guidelines for Port Structures, International Navigation Association (A.A. Balkema Publishers, Rotterdam, Netherlands).

Pina, F. E., Ventura, C. E., Taylor, G., & Finn, W. L. (2010, July). Selection of ground motions for the seismic risk assessment of low-rise school buildings in south-western British Columbia, Canada. In Proceedings of the Ninth US National and Tenth Canadian Conference on Earthquake Engineering, Toronto, Ont (pp. 25-26).

Port of Long Beach Wharf Design Criteria (2012). Version 3.0, February 29, , Los Anglese, USA.

Reese, L. and M. O'Neill (1987). Drilled shafts: Construction procedures and design methods. Federal Highway Administration, US Department of Transportation, McLean, Va, Report FHWA-HI-88-042.

Reese, L. C. and W. F. Van Impe (2010). Single piles and pile groups under lateral loading, CRC press.

Rogers, G., Halchuk, S., Adams, J., & Allen, T. (2015). 5th Generation (2015) seismic hazard model for southwest British Columbia. In 11th Canadian Conference on Earthquake Engineering (pp. 21-24).

Serventi, G. M., Jordan, M. A., Fotinos, G., & Soderberg, E. G. (2004). The Design of Earthquake Damage Repairs to Wharves Before the Earthquake Occurs. In Ports 2004: Port Development in the Changing World (pp. 1-10).

Shafieezadeh, A. (2011). Seismic vulnerability assessment of wharf structures. (PhD diss), Georgia Institute of Technology,

Shafieezadeh, A., DesRoches, R., Rix, G. J., and Werner, S. D.. (2012) "Seismic performance of pile-supported wharf structures considering soil-structure interaction in liquefied soil." Earthquake Spectra 28, no. 2: 729-757.

Shafieezadeh, A., DesRoches, R., Werner, S. D., and Rix, G. J.. (2009) "Seismic response of pile-supported container wharves." In TCLEE 2009: Lifeline earthquake engineering in a multihazard environment, pp. 1-10.

Shafieezadeh, A, DesRoches, R, Rix, G. J., and Werner, S. D. "Three-dimensional wharf response to far-field and impulsive near-field ground motions in liquefiable soils." Journal of Structural Engineering 139, no. 8 (2013): 1395-1407.

Smith, D., Naesgaard, E., & Kullmann, H. (2004, August). Seismic design of a new pile and deck structure adjacent to existing caissons founded on potentially liquefiable ground in Vancouver, BC. In Proceedings of 13th World Conference on Earhtquake Engineering, Vancouver, BC, Canada.

Strong-motion seismograph networks (K-NET, KiK-net). http://www.kyoshin.bosai.go.jp

StructurExpress. (2020). SE::Pile – Prestressed Concrete Pile Design. V2015.06.01.

Su, L., Lu, J., Elgamal, A., & Arulmoli, A. K. (2017). Seismic performance of a pile-supported wharf: Three-dimensional finite element simulation. Soil Dynamics and Earthquake Engineering, 95, 167-179.

Su, L., Wan, H. P., Dong, Y., Frangopol, D. M., & Ling, X. Z. (2019). Seismic fragility assessment of large-scale pile-supported wharf structures considering soil-pile interaction. Engineering Structures, 186, 270-281.

Terzic, V. (2011). "Force-based element vs. Displacement-based element."

Unified Facilities Criteria (UFC) (2005). Design: Piers and Wharves.

United States Geological Survey (2020) Earthquakes Data: https://earthquake.usgs.gov

Werner, S. and W. Cook (2010). "Wharf repair estimates for use in demonstration seismic risk analysis of port systems." Seismic Systems & Engineering Consultants, Oakland, CA.

Werner, S., McCullough, N., Bruin, W., Augustine, A., Rix, G., Crowder, B., & Tomblin, J. (2011). Seismic performance of Port de Port-au-Prince during the Haiti earthquake and post-earthquake restoration of cargo throughput. Earthquake Spectra, 27(1_suppl1), 387-410.

Werner, S. D., G. J. Rix, and R. DesRoches. (2008) "Seismic risk management for seaports." In 14th World Conference on Earthquake Engineering, Beijing, China.

Yang, C. S. W., DesRoches, R., & Rix, G. J. (2012). Numerical fragility analysis of vertical-pile-supported wharves in the western United States. Journal of Earthquake Engineering, 16(4), 579-594.

Appendix A. Seismic Design of a Wharf

A. 1. Wharf Structure Descriptions

The wharf analyzed in this project is a concrete pile-supported wharf, commonly used in container ports. It is assumed to be located in Vancouver harbor. The wharf profile is cited from the reference (Yang et al. 2012) (Figure A-1). The wharf has 8 piles (A, B, C, D, E, F, G and F) along its transverse direction (37.2 m long).

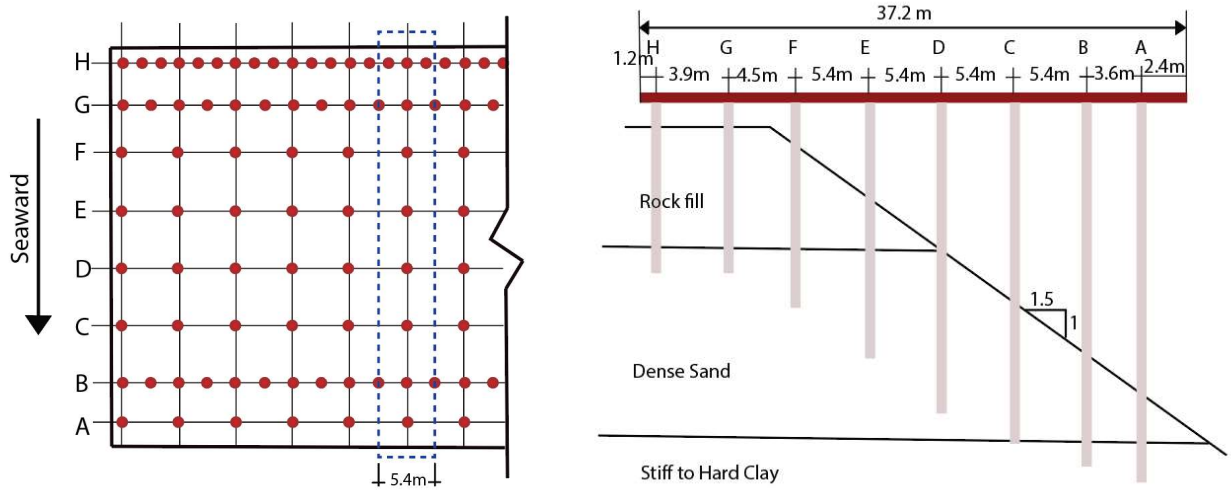

(a) (b)

Figure A-1 Profile of a wharf: a) plan view; b) section view (Yang et al. 2012)

The same soil layers used by Yang et al. (2012) were adopted in this project (Figure A-1 (b)). Similar soil profiles were reported at different locations in Vancouver, for example, the soil profiles for the pile-supported wharf in Port of Vancouver (Cowdell et al. 2001) and Vancouver harbor (Smith et al. 2004). The soil profile consists of three layers. The first layer is filled with 10 m of rockfill; the second one is 13.5 m of dense to very dense sand, and the rest is stiff to hard clay. The soil properties are summarized in Table A-1.

Table A-1 Soil properties (Yang et al. 2012)

Layer	Soil Layer	Total unit weight ($\frac{kN}{m^3}$)	Effective friction angle ($^\circ$)	Undrained shear strength (kPa)	Shear strain at 50% shear stress	Drag coefficient	C[2]
1	Rock Fill	18.1	45	-[1]	-[1]	0.3	0.0
2	Dense to very dense sand	20.9	42	-[1]	-[1]	0.3	1.5
3	Stiff to hard clay	17.8	-[3]	95.7 at top, increasing by 6.4 kPa/m at depth.	0.02	0.3	1.5

(1) Rock and sand do not consider shear properties.
(2) Viscous damping coefficient to represent radiation damping effects. (Boulanger et al. 1999)
(3) Clay does not consider friction angle.

The materials used in the design procedure have been summarized in Table A-2.

Table A-2 Material properties used in the design

Concrete	Compressive strength = 41.4 MPa (6 ksi). Young modulus = 30.44 GPa Unit weight = 24 kN/m^3
prestressing Steel	ASTM A416 Grade 270 Yielding Stress = 1860 MPa (270 ksi) Young modulus = 196.5 GPa Unit weight = 78.5 kN/m^3
Dowel Steel	ASTM A706 Grade 60 Yielding Stress of 410 MPa (60 ksi) Young modulus = 210 GPa Unit weight = 78.5 kN/m^3

A. 2. Load Cases

In Canada, the design of wharf structures based on ASCE 61 (2014) is a common practice, since there is no Canadian guideline regarding design of port structures. Since the wharf is assumed to be located in Vancouver harbor, British Columbia Building Code (BCBC 2018) seismic spectrum was used for seismic force calculation. According to ASCE 61-14 (2014), gravity load and design load combination were calculated based on Unified Facilities Criteria (UFC 2005). The effect of mooring and berthing were not considered in this project since the seismic hazard in the west coast is assumed to be the dominant load. Hydrodynamic force and Buoyancy load were also ignored in this design (UFC 2005).

Dead Load

The dead load consists of the self-weight of the structure. The unit dead weight of materials considered in the design of wharves (POLB-WDC 2012) is presented in Table A-2.

Live Load

The analyzed wharf was assumed to be a container wharf. According to the Port of Long Beach Wharf Design Manual, this kind of wharves shall be designed for a uniform live load of 48 KPa (POLB-WDC 2012). The impact is not considered when the design for uniform loads (UFC 2005).

Seismic Loads

ASCE61-14 recommends that for force-based design, the seismic base shear, V_s, can be calculated based on building code equations. Based on BCBC 2018, seismic base shear equals to

$$V_s = S(T_s) \times \frac{I_E}{R} \times W_t$$

Where:

I_E is the structure importance factor. The wharf is regarded as the post-disaster importance, so I_E = 1.5;

W_t is the seismic weight of the structure;

R is response modification factor (Table A-3);

T_s is the fundamental lateral period of structure; and

$S(T_s)$ is the design spectral acceleration at the fundamental period of the structure.

Table A-3 Design Coefficients for Various Elements (ASCE 61 2014)

Ductile element	R	C_d
Solid prestressed concrete piles	2	2

According to ASCE61-14, the fundamental period of the structure, T_s, can be estimated using an analytical model (ASCE61 2014). Thus, the period of the wharf was determined by implementing the model analysis via OpenSees. The effects of soil-structure interaction were considered in accordance with Section 4.8 of ASCE61-14, using inelastic lateral soil (p-y) springs to represent soil resistance in the analysis.

The design was an iterative procedure that started with an initial assumption of piles with 0.6 m octagonal cross-section and a deck thickness of 0.6 m. After a few iterations, the final fundamental period of the wharf was set to be 0.26 sec. Only the last cycle results are discussed in this appendix. The value of the design spectrum at T_s, $S(T_s)$, was determined by linear interpolation. Table A-4 shows the seismic response spectrum values, S_a, for Vancouver harbor:

Table A-4 Seismic hazard data for selected locations - Vancouver harbor (49.289606, -123.111972) (NRC 2020)

Probability of eceedance	$\mathbf{S_a(0.2)}$	$\mathbf{S_a(0.5)}$	$\mathbf{S_a(1.0)}$	$\mathbf{S_a(2.0)}$	$\mathbf{S_a(5.0)}$	$\mathbf{S_a(10)}$	**PGA**	**PGV**
2%/50 years	0.831	0.738	0.417	0.253	0.080	0.028	0.361	0.542
10%/50 years	0.424	0.372	0.200	0.115	0.025	0.010	0.184	0.256
40%/50 years	0.187	0.155	0.078	0.042	0.009	0.003	0.080	0.096

Based on Table 4.1.8.4-A NBCC 2015, the soil type for dense to very dense soils is C, therefore no site factor modification is needed (BCBC 2018), i.e. S (T) equals to S_a(T). The design spectrum has been presented in Figure A-2.

$$\frac{S_a(0.5) - S(\mathrm{T}_s)}{0.5s - \mathrm{T}_s} = \frac{S_a(0.5) - S(0.2)}{0.5s - 0.2s}$$

$$\frac{0.738 - S(0.26)}{0.24s} = \frac{0.738 - 0.831}{0.3s} = -0.31/s$$

$$S_a(0.26) = 0.738 + 0.31/s \times 0.24s = 0.82$$

Seismic weight shall be considered as dead load plus 10% live load (Engineers) 2014). The minimum lateral earthquake design force, V_s, shall be calculated as the below:

$$V_s = S(T_s) \times \frac{I_E}{R} \times W_t = 0.82 \times \frac{1.5}{2} \times W_t = 0.62W_t$$

The seismic weight of the structure considering dead load plus 10% design live load:

$W_t = A(D + 0.1L) = (5.4m \times 37.2m) \times (0.6m \times 24kN/m3 + 0.1 \times 48kPa) = 3859\ KN.$

$V_s = 0.62 \times 3859\ KN = 2391\ KN$

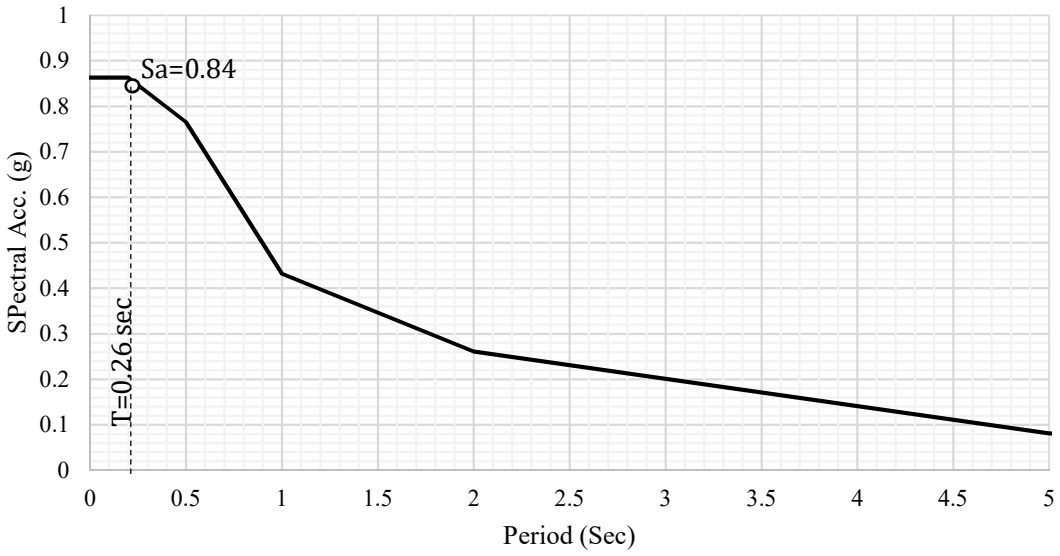

Figure A-2 Seismic Design Spectrum Vancouver harbor, BC-Site Class C

Load Combination

According to ASCE61-14, load combination considered in this project include:

$$(1+0.5*PGA)\ D+ 0.1L+ EQ \qquad \text{(Eq. A-1)}$$

Where D is the dead load of the structure, L is the live load, and EQ is the seismic force. PGA is peak ground acceleration.

A. 3. Design Procedure

There are two design procedures permitted by ASCE61-14, displacement-based and force-based design methods. The displacement-based design is applicable for all design classifications. The force-based design is permitted only for low design classification, and all other design classifications when $S_{DS} < 0.33$, where S_{DS} is design, 5 percent damped, spectral response acceleration parameter at short periods, Article 11.4 of ASCE7 (2016). In this project, the force-based design was used at first to generate the input for the numerical model, and displacement design was used to refine and verify the force-based design detail.

A. 4. Force-Based Design

Pile Forces

The pile forces were determined by linear static analysis of an Opensees model under the design load combination. Figure A- 3 Locations of pile forces recorded to show the locations that pile forces are recorded at and used for design purposes. The force at the top of the pile is used to design the pile-deck connections. The pile tip forces are used for load-bearing control of soil. The maximum cross-section forces along the pile were also recorded for the design of the pile itself. The piles' forces at different sections are presented in Table A-5 .

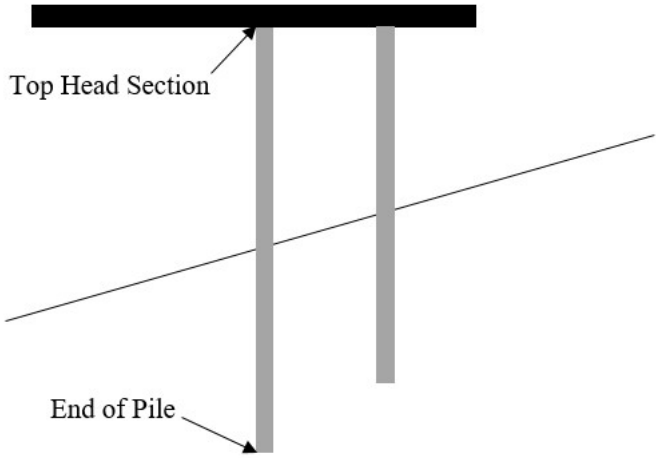

Figure A- 3 Locations of pile forces recorded

Table A-5 Piles sections forces

Pile Number	Top Head		Pile body maximum		Pile tip
	Axial (KN)	Moment (KN.m)	Axial (KN)	Moment (KN.m)	Axial (KN)
Pile A	2076	94	2075	82	2075
Pile B (2 Piles)(1)	2046	104	2044	95	2044
Pile C	2011	127	2008	125	2008
Pile D	1954	162	1950	175	1949
Pile E	1881	192	1874	172	1872
Pile F	1869	417	1878	367	1861
Pile G (2 Piles) (1)	1990	603	1983	456	1982
Pile H (3 Piles) (1)	1991	608	1984	451	1982

(1) The forces are for all piles.

Preliminary Structural Design

T-headed dowel connections were employed to connect precast piles to the top deck in this project. Figure A-4 shows the general detail of this type of connections.

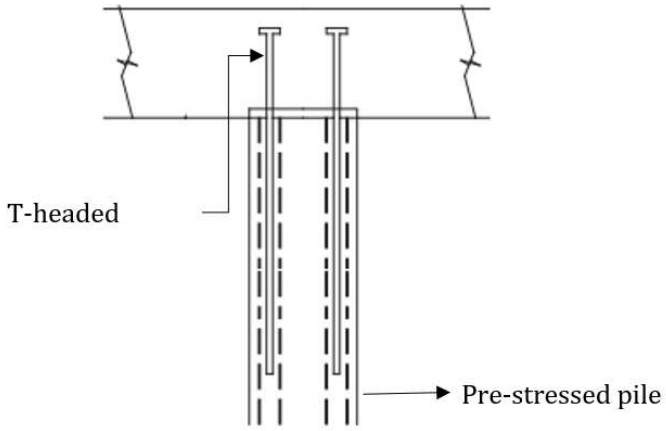

Figure A- 4 Connection typical detail

For piles A~F, there were 6-#8 (Nominal diameter of 25.4 mm and nominal area of 509 mm^2) welded head dowel rebars and for piles G & H, there were 6-#10 (Nominal diameter of 32.26 mm and nominal area of 819 mm^2) welded head rebars in the connections. The extended length of these rebars were 1.8 m and 2.2 m for #8 and #10 bars respectively. The octagonal section with a diameter of 0.61 m and 12 prestressing strands is shown in Figure A-6. The strand diameter was designed to be 15.24 mm with an area of 139 mm^2. A constant pretensioned force of 80 KN/m^2 has been applied for all piles. SE-PILE software (StructurExpress) was utilized to develop P-M interaction curves (Figures A-7 and A-8).

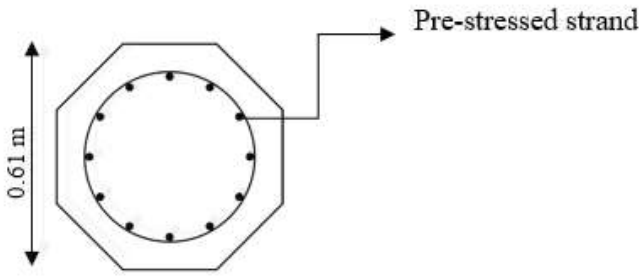

Figure A-5 General Section: (12 prestressed strand)

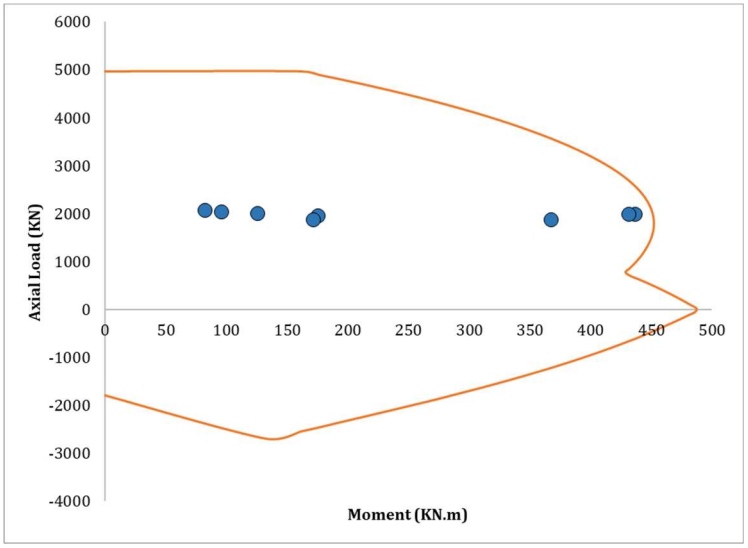

Figure A-6 P-M interaction curves for piles body

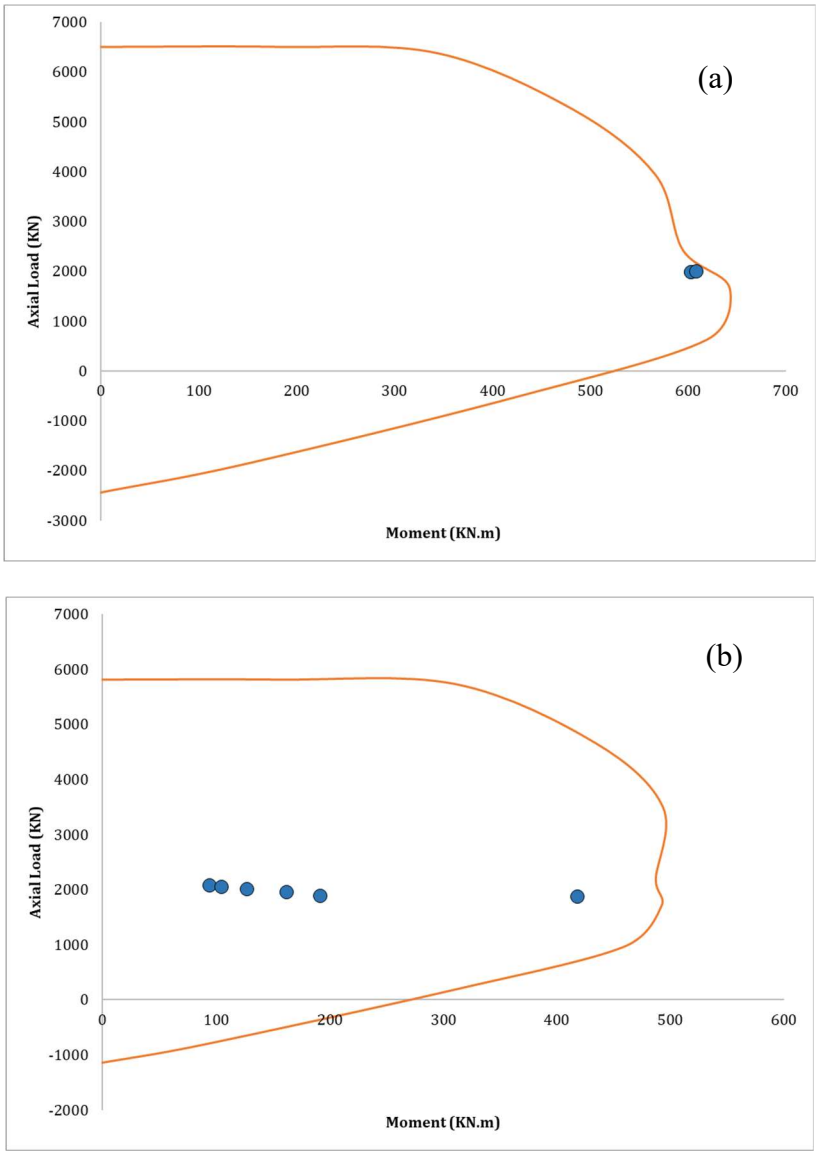

Figure A-7 P-M interaction curves of pile head; a) piles G&H, and b) piles A~F

Geotechnical Design of Piles

The ultimate bearing capacity of piles Q_d is determined based on (API 2002). The total ultimate bearing capacity of a pile is:

$$\boldsymbol{Q_d = Q_f + Q_p = fA_s + qA_p} \quad \text{(Eq. A-2)}$$

Where:

Q_f = skin friction resistance (kN)

Q_p = total end bearing (kN)

f = unit skin friction capacity (kPa)

A_s = side surface area of pile (m^2), for an octagonal section equals to $8\frac{\sqrt{2}}{2+\sqrt{2}}LD$

L= length of pile (m)

D= depth of pile section (m)

q = unit end bearing capacity (kPa)

A_p = gross end area of piles (m^2)

For octagonal piles with $D = 0.61\ m$: $A_p = 0.2924\ m^2$

For cohesive soil and clay:

q = 9c (API 2002):

c= undrained shear strength of the soil at the point in question (Table?).

$q = 9c = 9 \times 100\ kpa = 900\ kpa$

For Piles A to C $Q_p = 0.2924\ \times 900\ Kpa = \mathbf{263\ kN}$

For cohesionless soils like sand:

$$\boldsymbol{q = p_0 N_q} \quad \text{(Eq. A-3)}$$

Where:

p_0= overburden pressure at the pile tip (kPa)

N_q= dimensionless bearing capacity factor

Table A-6 Design Parameters for Cohesionless Soil (API 2002)

Density	Soil Description	Soil-Pile Friction Angle, $\boldsymbol{\delta}$ Degrees	Limiting Skin Friction Values (kPa)	$\boldsymbol{N_q}$	Limiting Unit End Bearing Values (MPa)
Dense	Sand	30	95.7	40	9.6

For dense sand $N_q = 40$ and overburden presure for a depth of h=10m:

$$q = p_0 N_q = (\gamma - \gamma_w).h.N_q = (20-10)\frac{kN}{m^3} \times 10m \times 40 = 4000\ \frac{KN}{m^2} = 4\ Mpa$$
$$< 9.6Mpa\ (Table\ A-7)$$

Where:

γ = Unit weight of soil ($\frac{kN}{m^3}$)

γ_w = Unit weight of water ($\frac{kN}{m^3}$)

$\boldsymbol{For\ Piles\ D\ to\ H}$: $Q_p = A_p q = 0.2924\ m^2 \times 4000\ \frac{KN}{m^2} = \mathbf{1169\ KN}$

Skin friction capacity in cohesive soil:

$$\boldsymbol{f = \alpha\, c} \qquad \text{(Eq. A-4)}$$

Where:

α= a dimensionless factor,

c= average undrained shear strength of the soil. (Table A-1)

The factor α can be computed by the Eq. A-5 and A-6:

$$\boldsymbol{\alpha = 0.5\Psi^{-0.5}, \Psi \leq 1.0} \quad \text{(Eq. A-5)}$$

$$\boldsymbol{\alpha = 0.5\Psi^{-0.25}, \Psi > 1.0} \quad \text{(Eq. A-6)}$$

$\Psi = c/\mathrm{p}_0'$ for the point of interest,

p_0'= effective overburden pressure at the pint of interest (kPa).

$$Q_f = fA_s = \alpha.c.A_s = 0.5\Psi^{-0.5}c.A_s = 0.5\left(\frac{\mathrm{c}}{p_0'}\right)^{-0.5} c.A_s = 0.5\left(\frac{\mathrm{c}}{(\gamma - \gamma_w).h}\right)^{-0.5} c.A_s$$

$h =$ Height of soil above the point of interest (m)

For the segments of piles A to C that are embedded in clay soil:

$$\boldsymbol{Pile\ C}: Q_f = 0.5\left(\frac{100\ \text{kpa}}{(200-100)\times 11.5}\right)^{-0.5} \times 100 \times 4.5 \times 8 \times \frac{\sqrt{2}}{2+\sqrt{2}} \times 0.61 = 1542\ KN$$

$$\boldsymbol{Pile\ B}: Q_f = 0.5\left(\frac{100\ \text{kpa}}{(200-100)\times 9.45}\right)^{-0.5} \times 100 \times 5.5 \times 8 \times \frac{\sqrt{2}}{2+\sqrt{2}} \times 0.61 = 1709\ KN$$

$$\boldsymbol{Pile\ A}: Q_f = 0.5\left(\frac{100\ \text{kpa}}{(200-100)\times 8}\right)^{-0.5} \times 100 \times 8.5 \times 8 \times \frac{\sqrt{2}}{2+\sqrt{2}} \times 0.61 = 2423\ KN$$

For sand and rock fill layers c equals to zero. The friction shall be calculated by Eq. A-7:

$$\boldsymbol{f = Kp_0\ tan\delta} \quad \text{(Eq. A-7)}$$

Where:

K= coefficient of lateral earth pressure

p_0= effective overburden pressure (kPa)

δ= friction angle between the soil and pile wall (Table A-7)

For low displacement driven pile: $K = 1.2K_0 = 1.2 \times (1 - sin\emptyset)$

$$Q_f = Ktan\delta p_0 A_s$$

$$= 1.2 \times (1 - \sin 45) \times \tan(30) \times ((\gamma - \gamma_w).h)_{ave} \times 8 \times \frac{\sqrt{2}}{2+\sqrt{2}} \times 0.61 \times L$$

$1.2 \times (1 - \sin 45) \times \tan(30) = 0.235$

Total length of piles D to H is located in sandy soil, thus:

$\boldsymbol{Pile\ G}$ & $\boldsymbol{H}$: $Q_f = 0.235 \times (0.5 \times 20 \times 11.75) \times 8 \times \frac{\sqrt{2}}{2+\sqrt{2}} \times 0.61 \times 11.75 = 656\ KN$

$\boldsymbol{Pile\ F}:\ Q_f = 0.235 \times (0.5 \times 20 \times 12.6) \times 8 \times \frac{\sqrt{2}}{2+\sqrt{2}} \times 0.61 \times 12.6 = 754\ KN$

$\boldsymbol{Pile\ E}$: $Q_f = 0.235 \times (0.5 \times 20 \times 13) \times 8 \times \frac{\sqrt{2}}{2+\sqrt{2}} \times 0.61 \times 13 = 684\ KN$

$\boldsymbol{Pile\ D}$: $Q_f = 0.235 \times (0.5 \times 20 \times 13.4) \times 8 \times \frac{\sqrt{2}}{2+\sqrt{2}} \times 0.61 \times 13.4 = 852\ KN$

For the segments of piles A to C that are embedded in sandy soil:

$\boldsymbol{Pile\ A}$: $Q_f = 0.235 \times (0.5 \times 20 \times 4.3) \times 8 \times \frac{\sqrt{2}}{2+\sqrt{2}} \times 0.61 \times 4.3 = 88\ KN$

$$\textbf{\textit{Pile B}}: Q_f = 0.235 \times (0.5 \times 20 \times 6.7) \times 8 \times \frac{\sqrt{2}}{2+\sqrt{2}} \times 0.61 \times 6.7 = 231\ KN$$

$$\textbf{\textit{Pile C}}: Q_f = 0.235 \times (0.5 \times 20 \times 10.3) \times 8 \times \frac{\sqrt{2}}{2+\sqrt{2}} \times 0.61 \times 10.3 = 504\ KN$$

Table A- 7 Pile geotechnical capacities

Pile Number	Total length	End Elev.	Soil Surface Elev.	length in cohesionless soil	length in cohesive soil	Q_p	Q_f	Q_t	Pile tip force
A	32	-32	-19.2	4.3	8.5	263	88+2423	2774	2075
B	29	-29	-16.8	6.7	5.5	263	231+1709	2203	2014
C	28	-28	-13.2	10.3	4.5	263	504+1542	2309	2008
D	23	-23	-9.6	13.4	-	1169	852	2021	1949
E	19	-19	-6	13	-	1169	802	1970	1873
F	15	-15	-2.4	12.6	-	1169	754	1923	1861
G	13	-13	-1.25	11.75	-	1169	656	2*1825	1982
H	13	-13	-1.25	11.75	-	1169	656	3*1825	1983

A. 5. Displacement-Based Design

For displacement-based design, three design classifications are defined by ASCE61: High, Moderate, and Low. Since the wharf structure is essential to the region's economy and post-disaster recovery, the design classification is assumed as High. The expected performance level for different seismic hazard levels is presented in Table A-8. Each performance level has its relevant strain limit of structural components which will be discussed in Table A-9.

Table A-8 Minimum Seismic Hazard and Performance Requirements (ASCE 61 2014)

	Seismic hazard level and performance level					
	Operating level earthquake (OLE)		Contingency level earthquake (CLE)		Design earthquake (DE)	
	Ground motion probability of exceedance	Performance level	Ground motion probability of exceedance	Performance level	Ground motion probability of exceedance	Performance level
High	50% in 50 years (72-year return period)	Minimal damage	10% in 50 years (475-year return period)	Controlled and repairable damage	Design earthquake(1)	Life safety protection

(1) In NBCC, it is 2% in 50 years.

Structural Design of Piles

Figure A-8 shows the procedure of a displacement-based design approach. The procedure presented in ASCE-61 is more comprehensive. However, in this project, a fiber section was used for the nonlinear model created in OpenSees. The strain of concrete and steel at different locations along the piles can be reordered directly and compared to the damage state criteria (strain limits at Operation level earthquake (OLE), Contingency level earthquake (CLE), and design level earthquake (DE)) (Engineers) 2014).

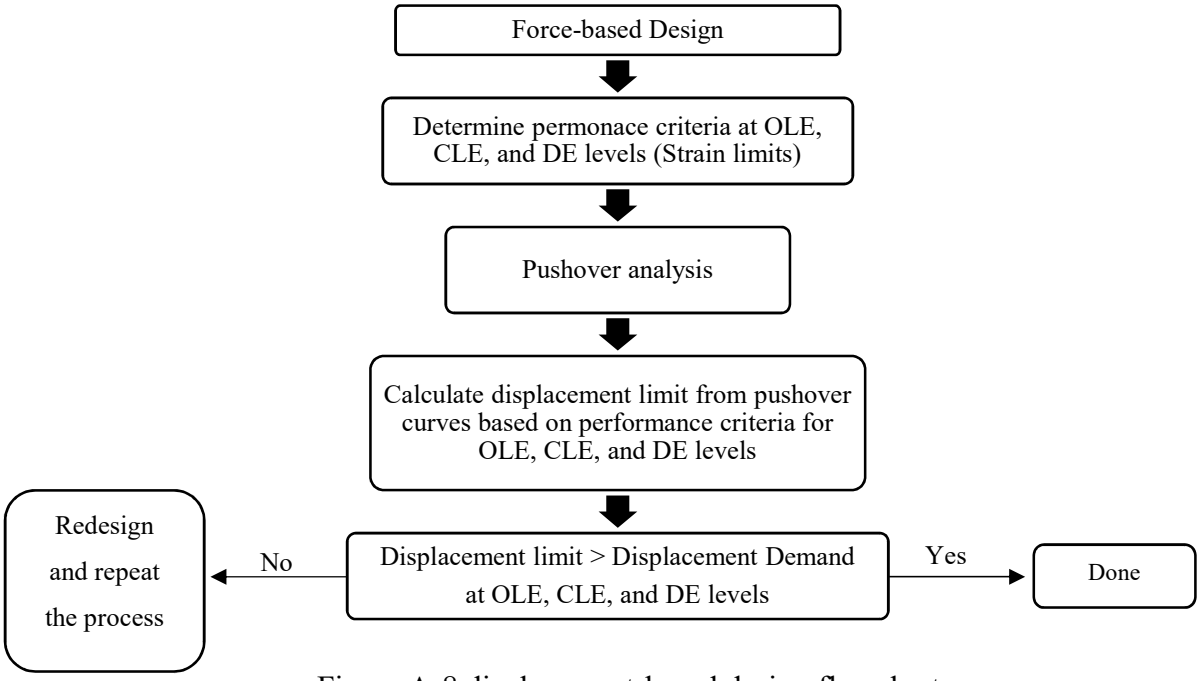

Figure A-8 displacement-based design flowchart

Displacement capacity shall be based on the pile strain limits, which the nonlinear pushover method was used to calculate. Therefore, the response of structure at a different level of earthquake can be achieved by performing nonlinear pushover analyses. Figure A-10 shows the pushover curve of the structure. The bilinear approximation of the pushover curve has been estimated using an equal energy approach (Engineers) 2014). In this method, two lines are implemented; the first one is a line tangent to the linear part of the curve, and the second one is a line ending in strength loss point and with an adjusted slope somehow that the idealized bilinear and the original curves provide equal energy. The intersection of these two curves gives the yield point.

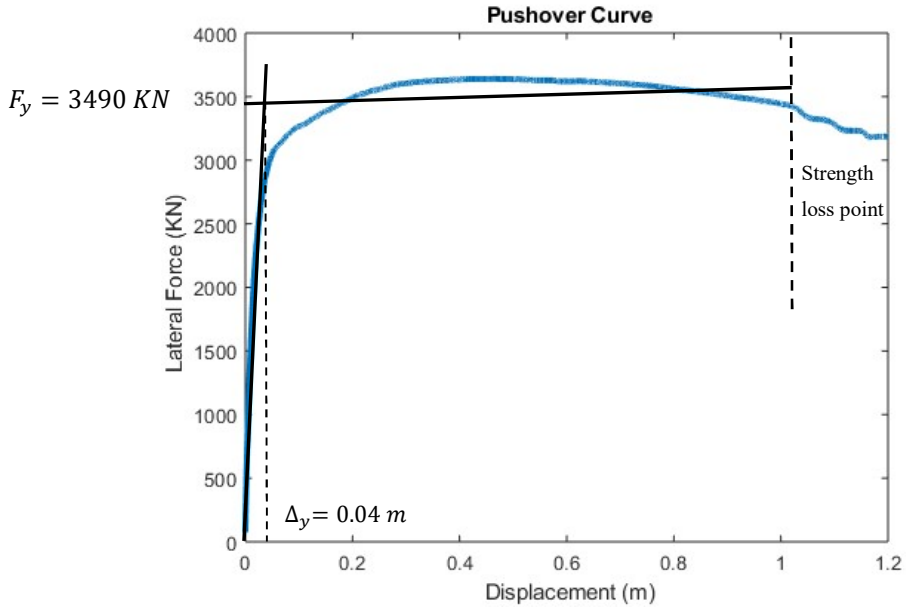

Figure A-9 Pushover curve of the wharf structure

Calculating Piles Displacement Capacity for OLE, CLE, and DE

ASCE 61 (2014) provides seismic design criteria for the design of port structures such as piers and wharves. In this standard, displacement-based design is introduced as one of the most reliable design procedures, as it allows engineers to determine the level of damage of ports developed in different seismic intensities. Three performance levels are defined in the standard: Minimal Damage, Controlled or Repairable Damage, and Life Safety Protection.

- **Minimal Damage (Serviceability):** A structure shall be classified as having achieved "minimal damage" when (a) it exhibits near elastic structural response with minor or no residual deformation, (b) there is no loss of serviceability of the structure, and (c) there is no loss of containment of materials in a manner that would pose a public hazard (ASCE61-14).
- **Controlled and Repairable Damage:** A structure shall be classified as having achieved "controlled and repairable damage" when (a) the structure responds in a controlled and ductile manner, experiencing limited inelastic deformations at locations where repair is possible; (b) the required repairs result in a loss of serviceability for no more than several months; and (c) there is no loss of containment of materials in a manner that would pose a public hazard (ASCE61-14).

- **Lie Safety Protection (Severe damage):** A structure shall be classified as providing "life safety protection" when (a) the post-earthquake damage state is such that the structure continues to support gravity loads, (b) damage that does occur does not prevent egress, and (c) there is no loss of containment of materials in a manner that would pose a public hazard (ASCE 61-14).

Pile displacement limits at different levels of seismic hazard, OLE, CLE, and DE can be determined using OpenSees pushover analysis based on the strain limits of components provided in Table A-9. The displacement limit refers to the smallest horizontal displacement at which the strain in any part of the pile reaches the limit states shown in Table A-9.

Table A- 9 Strain Limits (POLB-WDC 2012)

	Component	Top of pile	In-ground	Deep in ground (> 10 **Dp**)
Minimal Damage	Concrete	$\varepsilon_c \leq 0.005$(1)	$\varepsilon_c \leq 0.005$	$\varepsilon_c \leq 0.008$
	Reinforcing steel	$\varepsilon_s \leq 0.015$(2)	-	-
	prestressing steel	-	$\varepsilon_p \leq 0.015$(4)	$\varepsilon_p \leq 0.015$
Controlled and Repairable Damage	Concrete	$\varepsilon_c \leq 0.005 + 1.1\rho_s \leq 0.025$	$\varepsilon_c \leq 0.005 + 1.1\rho_s \leq 0.008$	$\varepsilon_c \leq 0.012$
	Reinforcing steel	$\varepsilon_s \leq 0.6\varepsilon_{smd} \leq 0.06$ (3)	-	-
	prestressing steel	-	$\varepsilon_p \leq 0.025$	$\varepsilon_p \leq 0.025$
Life Safety Protection	Concrete	-	$\varepsilon_c \leq 0.005 + 1.1\rho_s \leq 0.012$ (5)	-
	Reinforcing steel	$\varepsilon_s \leq 0.8\varepsilon_{smd} \leq 0.08$	-	-
	prestressing steel	-	$\varepsilon_p \leq 0.035$	$\varepsilon_p \leq 0.050$

(1) ε_c is extreme concrete fiber compressive strain;
(2) ε_s is regular strain;
(3) ε_{smd} is the strain at peak stress of dowel reinforcement as specified in Figure A

(4) ε_p is strain in prestressing tendons;
(5) ρ_s is volumetric ratio of confining steel;
(6) D_p is the pile's diameter.

Based on ASCE 61(2014), strain at peak stress of dowel reinforcement, ε_{smd}, equals 0.12 for #10 and smaller bars and 0.09 for #11 and larger bars.

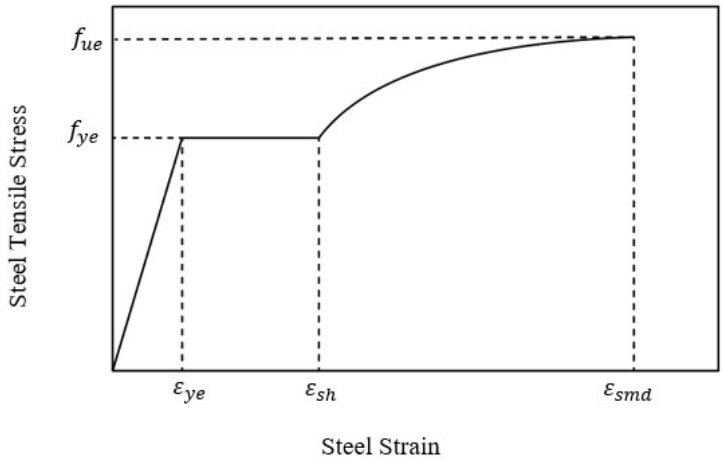

Figure A-10 Stress-strain relationship for reinforcing steel (Port of Long Beach 2012)

Based on pushover analysis, it was noticed that the shorter piles, G and H, would reach the strain limit state earlier than other piles, so controlled the lateral displacement limit of the wharf. For the OLE seismic level, the displacement limit is based on concrete strain limits at top of piles G and H which equals 0.019 m. For the CLE level, the displacement limit is 0.067 m. For DE level, the displacement limit is based on rebar strain limits at the top of piles G and H which equals 0.435 m.

Calculating Displacement Demand

Figure A-11 shows the procedure proposed by the Port of Long Beach Design Manual (POLB-WDC 2012) to calculate the displacement using the Elastic Stiffness Method. In this method, it is necessary to calculate the spectral displacement from 5% damped response spectrum for OLE, CLE and DE levels (ASCE61- EQ6.15).

$$\Delta_t = S_A \frac{T^2}{4\pi^2} \quad \text{(Eq. A-8)}$$

Where

Δ_t is the transverse displacement demand;

S_A is spectral response acceleration at the period of T.

To calculate the period of T, it is crucial to calculate the effective secant stiffness, K_{eff}, from the pushover curve (Figure A-10) based on Article 6.8.3 of ASCE61-14. K_{eff} equals to the initial stiffness, K_i, when demand displacement is less than the first yield of the structure or soil, its yield displacement was calculated from Figure A-10. When demand displacements exceed this first yield, K_{eff} is determined at the demand displacement. T can be calculated as:

$$T = 2\pi \sqrt{\frac{m}{K_{eff}}} \quad \text{(Eq. A-9)}$$

Where m is mass of the structure.

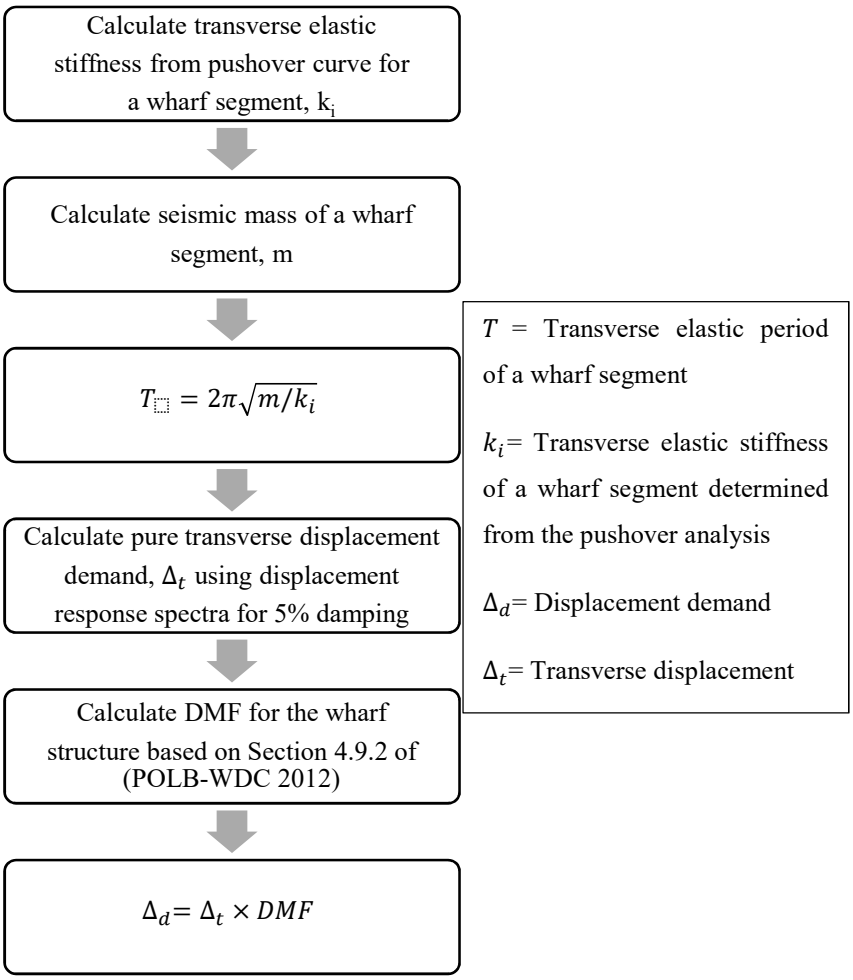

Figure A-11 Flow Diagram for the Elastic Stiffness Method (POLB-WDC 2012)

Calculate initial stiffness of structure from pushover curve (Figure A-8):

$F_y = 3490\ KN$

$\Delta_y = 0.04\ m$

$K_i = \frac{3490}{0.04} = 87250\ KN/m$

The seismic mass of the structure (dead load + 10% design live load) equals to $393\ KN.sec^2/m$. Then the period (ASCE61- EQ6.14) based on initial stiffness will be:

$$T = 2\pi\sqrt{\frac{393\ KN.sec^2/m}{87250\ KN/m}} = 0.42\ sec$$

Spectral acceleration at the period of 0.42 sec is 0.791g, 0.386g, and 0.163g for probability of 2%, 10%, and 40% in 50 years, respectively.

DMF is Dynamic magnification factor (DMF): The seaward piles have less lateral stiffness, creating eccentricity between the center of mass and the effective center of rigidity of the wharf, which will induce torsional response in the structure under longitudinal excitation. In this case, a Dynamic Magnification Factor of 1.1 is multiplied to account for torsional response.

For DE (2% in 50 years) earthquake $\Delta_t = 0.791\text{g} \times \frac{0.42^2}{4\pi^2} = 0.035$ m

$\Delta_t = \text{DMF}.\Delta_t = 1.1 \times 0.035 = 0.0381$ m < 0.435m

For CLE (10% in 50 years) earthquake $\Delta_t = 0.386\text{g} \times \frac{0.42^2}{4\pi^2} = 0.017$ m

$\Delta_t = \text{DMF}.\Delta_t = 1.1 \times 0.017 = 0.019$ m < 0.067m

Since the seismic hazard for the probability of 50% in 50 years is not available in NRC calculator tool, conservatively, probability of 40% in 50 years is considered for OLE hazard level.

For OLE (50% in 50 years) earthquake $\Delta_t = 0.163\text{g} \times \frac{0.42^2}{4\pi^2} = 0.007$ m

$\Delta_t = \text{DMF}.\Delta_t = 1.1 \times 0.007 = 0.008$ m < 0.019m

As it can be seen, the demand displacement at different seismic hazard levels are less than the displacement limit, so the structure passes the performance level criteria.

A. 6. Deck Design

Here, in terms of flexural reinforcement and shear capacity, the sufficiency of the depth of the deck is controlled. It worth noting that the reinforcement of the deck is not considered in the numerical modeling. The deck is a capacity-protected member, so the design forces shall be determined from an amplified moment, M_{pa}, based on the moment at pile plastic hinges (Engineers) 2014):

$$\boldsymbol{M_{pa} = 1.25 M_p} \qquad \text{(Eq. A-9)}$$

M_p is the plastic moment of the pile from moment-curvature analysis via OpenSees as shown in Figure A-12, and M_{pa} should be used for capacity control of the deck.

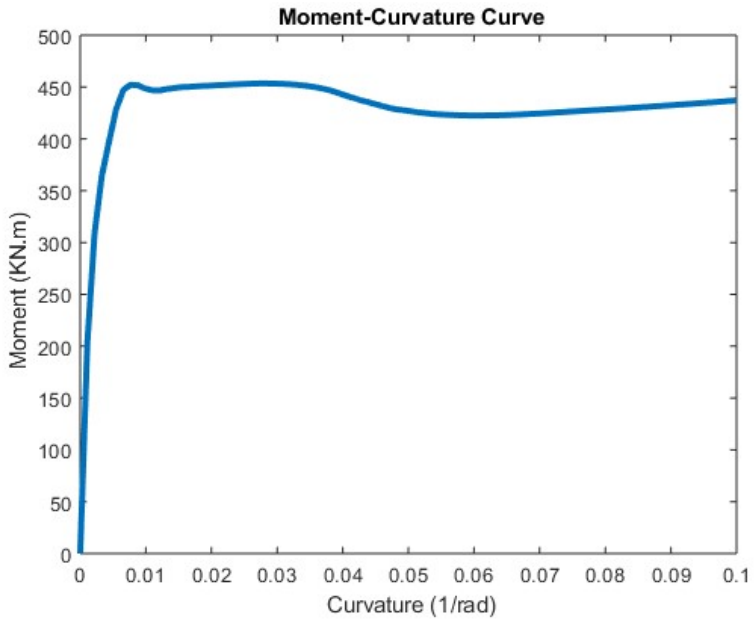

Figure A-12 Moment-Curvature of pile A to F section

From Moment-Curvature analysis of section:

$M_p \approx 450\ KN.m$

$M_{pa} = 1.25 M_p = 562.5\ KN.m$

The bending strength of piles has been replaced by amplified plastic moment and has been analyzed in SAP2000 software. The deck modeled using shell elements with a uniform dead and live load

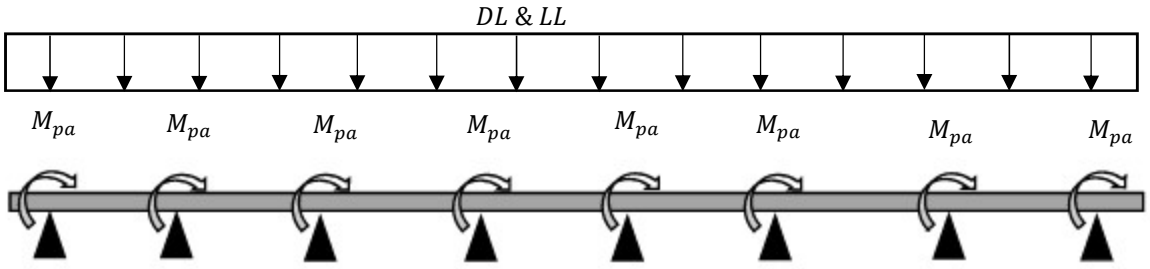

Figure A-13 Applied loads on deck in SAP2000

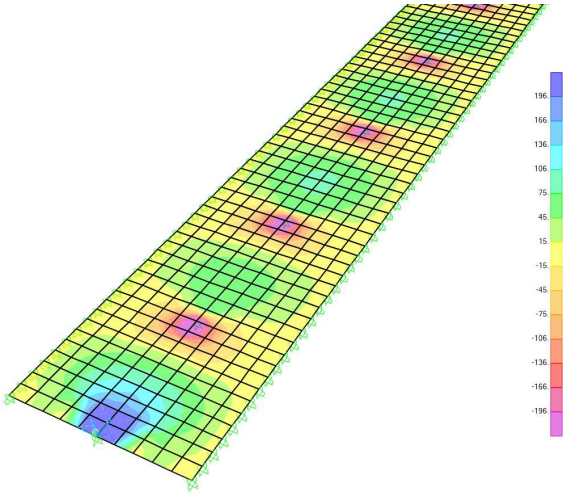

Figure A-14 Moment distribution in deck (KN.m/m)- M_{max}=590 KN.m/m

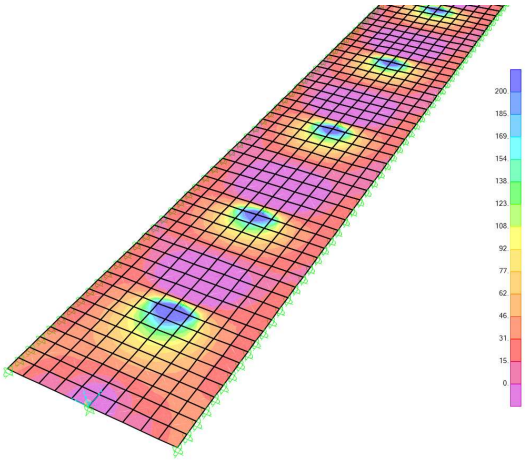

Figure A-15 Shear distribution in deck (KN/m)- V_{max}=450 KN/m

Flexural Capacity of Deck:

A depth of 600 mm reinforced concrete slab has been used here. Based on CSA A23.3, a minimum area of reinforcement, A_{smin}, of 0.002A_g shall be provided in each direction. For 1m width: $A_{smin} = 1200\ mm^2$

Assuming the section is under-reinforced, and $A_s = 8000\ mm^2$ per unit width:

$$\boldsymbol{a = \frac{\varphi_s . f_y . A_s}{\alpha_1 . \varphi_c . f_c . b}} \qquad \text{(Eq. A-10)}$$

Where:

A_g = gross section area

a= depth of equivalent rectangular stress block

A_s = area of longitudinal reinforcement on the flexural tension side of the member

A_{smin}= minimum area of tension reinforcement

φ_c= resistance factor for concrete

φ_s= resistance factor for rebars

f_c= specified compressive strength of concrete

f_y= specified yield strength of non-prestressed reinforcement or anchor steel

α_1= ratio of average stress in rectangular compression block to the specified concrete strength

$$a = \frac{\varphi_s . f_y . A_s}{\alpha_1 . \varphi_c . f_c . b} = \frac{0.85 \times 410 \times 8000}{0.85 \times 0.65 \times 41.4 \times 1000} = 122\ mm$$

The tensile force provided by rebar equals to Eq. A-11:

$$\boldsymbol{T_r = \varphi_s . f_y . A_s} \qquad \text{(Eq. A-11)}$$

$$T_r = 0.85 \times 410 \times 8000 = 2788k\ N$$

Resistance moment, M_r, can be calculated from Eq. A-12, and for 1 m of width equals to:

$$\boldsymbol{M_r = T_r \left(d - \frac{a}{2}\right)} \qquad \text{(Eq. A-12)}$$

$$M_r = T_r \left(d - \frac{a}{2}\right) = 2788000 \left(600 - 75 - \frac{122}{2}\right) = 1293\ KN.m\ > 581\ KN.m$$

Now the strain in steel should be checked since it was assumed the section is under-reinforced.

$$\frac{\beta_1 . a}{d} = \frac{0.0035}{0.0035 + \varepsilon_s} \rightarrow \varepsilon_s = 0.012\ > \varepsilon_y = 0.002\ Ok.$$

Where:

d= effective depth of section

β_1=ratio of depth of rectangular compression block to depth to the neutral axis

ε_y=yield strain in reinforcement

ε_s=strain in reinforcement

So, the capacity is more than demand, which means that design is acceptable.

Shear Capacity of Deck:

Here it is assumed that concrete only resist against shear.

$$\boldsymbol{V_c = \varphi_c \lambda \beta \sqrt{f'_c} b_w d_v} \quad \text{(Eq. A-13)}$$

$$\boldsymbol{V_s = \frac{\varphi_s A_v f_y d_v cot\theta}{s}} \quad \text{(Eq. A-14)}$$

Where:

V_c= shear resistance attributed to the concrete

V_s= shear resistance provided by shear reinforcement

λ= factor to account for low-density concrete,

b_w= beam web width or diameter of circular section or wall thickness

d_v= effective shear depth,

β= factor accounting for shear resistance of cracked concrete

A_v=area of shear reinforcement within a distance s

θ= angle of inclination of diagonal compressive stresses to the longitudinal axis of the member

s= maximum centre-to-centre spacing of transverse reinforcement

Per Clause 11.3.6 CSA A23.3, $\theta = 35$ and $\beta = 0.18$.

$d_v = \max(0.9d, 0.72h) = \max(0.9 \times (600 - 75), 0.72 \times 600) = 472.5\ mm$

Shear resistance provided by concrete for 1 meter of width:

$V_c = \varphi_c \lambda \beta \sqrt{f_c'} b_w d_v = 0.65 \times 1 \times 0.18 \times \sqrt{41.4} \times 1000 \times 472.5 = 276.4\ KN$

Since the provided shear capacity by concrete is not enough, shear reinforcement can be used in depth of 600 mm, assuming a spacing of 400mm:

$V_s = V_{max} - V_c = 553.2 - 276.4 = 276.8\ KN$

$$276.8\ KN = \frac{\varphi_s A_v f_y d_v cot\theta}{s} = \frac{0.85 \times A_v \times 400 \times 472.5 \times cot35}{400}$$

$A_v = 480\ mm^2$ for one meter width.